2 P (mix)

RF Project 2267
Report No. 15

THE OHIO STATE UNIVERSITY

RESEARCH FOUNDATION

1314 KINNEAR ROAD COLUMBUS, OHIO 43212

STRESS CORROSION CRACKING OF TITANIUM ALLOYS

G. R. Statler, J. W. Spretnak,
F. H. Beck and M. G. Fontana

Department of Metallurgical Engineering

1 July 1973 - 31 December 1973

NATIONAL AERONAUTICS AND SPACE ADMINISTRATION
Lewis Research Center
21000 Brookpark Road
Cleveland, Ohio 44135

Grant No. NGL-36-008-051

65

RF Project 2267

Report No. 15

SEMIANNUAL

REPORT

By

THE OHIO STATE UNIVERSITY
RESEARCH FOUNDATION

1314 KINNEAR RD.
COLUMBUS, OHIO 43212

To NATIONAL AERONAUTICS & SPACE ADMINISTRATION
Lewis Research Center
21000 Brookpark Road
Cleveland, Ohio 44135
Grant No. NGL-36-008-051

On STRESS CORROSION CRACKING OF TITANIUM ALLOYS

For the period 1 July 1973 - 31 December 1973

Submitted by G. R. Statler, J. W. Spretnak, F. H. Beck
and M. G. Fontana
Department of Metallurgical Engineering

Date June, 1974

FOREWORD

This report covers the work period July 1, 1973 through December 31, 1973, on THE EFFECT OF HYDROGEN ON PLASTIC INSTABILITIES IN TITANIUM.

This report is based on the M.S. Thesis of Mr. G. R. Statler. Professor J. W. Spretnak provided the mechanical metallurgy guidance essential to this research effort. The work was performed at The Ohio State University under NASA Grant No. NGL-36-008-051.

TABLE OF CONTENTS

	Page
INTRODUCTION	1
LITERATURE REVIEW	2
Titanium Stress Corrosion	2
Hydrogen in Titanium	4
Fracture of Metals	7
EXPERIMENTAL PROCEDURES	10
Alloy Ti-5Al-2.5Sn	10
Alloy Ti-8Al-1Mo-1V	16
RESULTS	19
Ti-5Al-2.5Sn Alloy	19
Ti-8Al-1Mo-1V Alloy	24
DISCUSSION	34
Ti-5Al-2.5Sn Alloy	34
Ti-8Al-1Mo-1V Alloy	40
CONCLUSIONS	52
RECOMMENDATIONS FOR FUTURE WORK	53
APPENDIX - SAMPLE CALCULATIONS FOR HYDROGENATION PROCEDURE	55
REFERENCES	57

LIST OF FIGURES

Figure		Page
1	The effect of applied potential on the velocity of cracking of Ti-8Al-1Mo-1V alloy in a neutral 3.5% NaCl solution	3
2	Interrelationship between stress intensity and dissolved hydrogen content	6
3	Sheet tensile specimen for Ti-5Al-2.5Sn	11
4	Diagram of hydrogenating system	13
5	Sheet tensile specimen for Ti-8Al-1Mo-1V	17
6	Fine grain structure on Ti-5Al-2.5Sn sheet containing 10 ppm hydrogen	20
7	True stress vs true strain for Ti-5Al-2.5Sn with strain rate 0.1575 min^{-1}	22
8	True stress vs true strain for Ti-5Al-2.5Sn with strain rate 0.1575 min^{-1}	23
9	Hydrides present in the Ti-5Al-2.5Sn alloy containing 500 ppm hydrogen	25
10	Fracture events for Ti-5Al-2.5Sn with 80 ppm hydrogen at 0.1575 min^{-1} strain rate	26
11	Vacuum annealed Ti-8Al-1Mo-1V alloy showing fine α grain size with islands of β phase	26
12	True stress vs true strain for Ti-8Al-1Mo-1V with strain rate 0.14 min^{-1}	28
13	True stress vs true strain for Ti-8Al-1Mo-1V with strain rate 0.14 min^{-1}	29
14	Fractures of Ti-8Al-1Mo-1V at 0.14 min^{-1} strain rate	31
15	Fractures of Ti-8Al-1Mo-1V at 0.14 min^{-1} strain rate	31
16	Fracture of aged Ti-8Al-1Mo-1V with strain rate of 0.14 min^{-1}	33
17	Log true stress vs log true strain for Ti-5Al-2.5Sn	35

Figure		Page
18	Strain parameters for Ti-5Al-2.5Sn with strain rate 0.1575 min^{-1}	36
19	Typical fracture pattern for separation at the center of a tensile specimen	37
20	Typical load-extension curve for Fig. 21 fracture	39
21	Void formation in a Ti-5Al-2.5Sn specimen related to particles in the grain boundaries	41
22	Strain parameters for Ti-8Al-1Mo-1V	42
23	Log true stress vs log true strain	45
24	Fracture surface of unaged Ti-8Al-1Mo-1V specimen containing 10 ppm hydrogen	47
25	Fracture surface of aged Ti-8Al Mo-1V specimen containing 10 ppm hydrogen	47
26	Schematic of Fig. 17A showing thick instability flow band and the pores nucleated in it	48
27	Schematic of the interaction of major deformation bands and the fracture pattern produced	51

LIST OF TABLES

Table		Page
I	Chemical Analysis of As-Received Titanium Sheet	10
II	Hydrogen Concentration of Selected Specimens	14
III	Ti-5Al-2.5Sn Alloy: True Stress and True Strain Data for a Strain Rate of 0.1575 Min^{-1}	21
IV	Strain Parameters for Ti-5Al-2.5Sn Alloy as Affected by Hydrogen Concentration	24
V	Ti-8Al-1Mo-1V Alloy: True Stress and True Strain Data for a Strain Rate of 0.140 Min^{-1}	27
VI	Strain Parameters as Affected by Hydrogen Concentration Ti-8Al-1Mo-1V Alloy	30
VII	Strain Parameters for Ti-8Al-1Mo-1V Aged to Produce Ti_3Al Compound	32
VIII	Strain Parameters for Ti-8Al-1Mo-1V as Affected by the Rolling Direction	32
IX	Comparison of Final Strain Using $\ln L/Lo$ and $\ln Ao/A$	43
X	Angles of Instability Formation	43
XI	Ti-8Al-1Mo-1V Ductility Data	44

THE EFFECT OF HYDROGEN ON PLASTIC INSTABILITIES IN TITANIUM

INTRODUCTION

The effect of hydrogen on the properties of metals, including titanium and its alloys, has been investigated for many years. Of the several basic means by which hydrogen can gain entry into titanium hydrogen generated during corrosion is the most important and is most discussed in the literature. In addition to generating hydrogen, corrosion is the primary means for sharpening the notch or crack, for increasing the stress intensity, for producing ions capable of adsorbing on the surface and absorbing into the lattice, and/or for producing surface films thought to be vital to stress corrosion.

It is believed that premature failure of titanium in a corrosive environment follows the basic mechanisms of normal fracture. Exceptions to this would be those cases in which the stress corrosion is known to occur solely by anodic dissolution (an electrochemical process). Therefore, it is of primary importance to understand fracture mechanisms if one is to understand stress-corrosion failures.

As a background for the present study the basic theories of stress corrosion of titanium alloys will be reviewed. Since hydrogen absorption seems to play a vital role in the stress-cor osion cracking process, an attempt will be made to review literature concerned with the effect of absorbed hydrogen on the mechanical properties of metals. Finally, the basic modes of metal fracture and their importance to this study will be considered.

The experimental work performed in this research was designed to determine the effects of hydrogen concentration on the critical strain at which plastic instability along pure shear directions occurs. The materials used were titanium alloys Ti-8Al-1Mo-1V and Ti-5Al-2.5Sn.

LITERATURE REVIEW

TITANIUM STRESS CORROSION

A number of variables have been associated with the stress corrosion of titanium. These include environment, electrochemical potential, stress, metallurgical structure, alloy content, surface films, and heat treatment.

Reduced notch fracture toughness has been reported for titanium in hot salt, nitrogen tetroxide, methanol, and salt water environments. Beck[1] found that Cl^-, Br^-, and I^- ions caused cracking and that the cations present were unimportant. He also observed that in an aqueous NaCl environment, as the potential was shifted in the active direction the crack velocity increased, while a shift in the negative direction caused the velocity to decrease until a point was reached at which the crack stopped propagating [~ -1000 mV (SCE)]. He reported this to mean that the mechanism was anodic dissolution dependent on the Cl^- ion mass transport. Powell and Scully[2] theorized that the OH^-/Cl^- ratio was critical and that at lower cathodic potentials the higher ratio caused a film formation which limited or eliminated ingress of hydrogen into the metal. Chen *et al.*[3] showed two areas of susceptibility in different concentrations of NaCl and KBr and showed that the propagation rate increased to about -500 mV (SHE) [~ -750 mV (SCE)] at which point the propagation decreased with increasing potential. Green and Sedricks[4] showed that the cracking velocity had two maximums for Ti-8-1-1 material in 3.5% NaCl solution and that the data agreed with that of Beck only in the region -800 to -200 mV (SCE) as shown in Fig. 1.

The stress state present is known to have an effect on the susceptibility of an alloy to stress-corrosion cracking. The procedural developments in fracture toughness testing have thus played an important role in the study of stress-corrosion cracking. Many authors are presently using stress intensity values at the onset of stress-corrosion cracking to compare titanium alloys for sensitivity. It is generally accepted that it is very difficult, if not in some cases impossible, to initiate cracking in titanium, thus most work has been done with a pre-existing crack; although Fontana *et al.*[5] demonstrated that initiation on smooth Ti-8-1-1 sheet in aqueous room temperature environments is possible. The triaxial tension state of a notch causes reduced ductility in the material tested and enhances those factors which lead to brittle-like failure.

The metallurgical structure as well as the alloy content have major roles in determining susceptibility. Lists have been compiled of those alloys susceptible in salt water,[6-10] generally alpha alloys are susceptible while alpha-beta alloys may or may not be. Stress-corrosion cracks in alpha-beta alloys normally follow the alpha phase or the interface. The alpha stabilizer, aluminum, has a marked effect on susceptibility. There is a transition to susceptibility at about

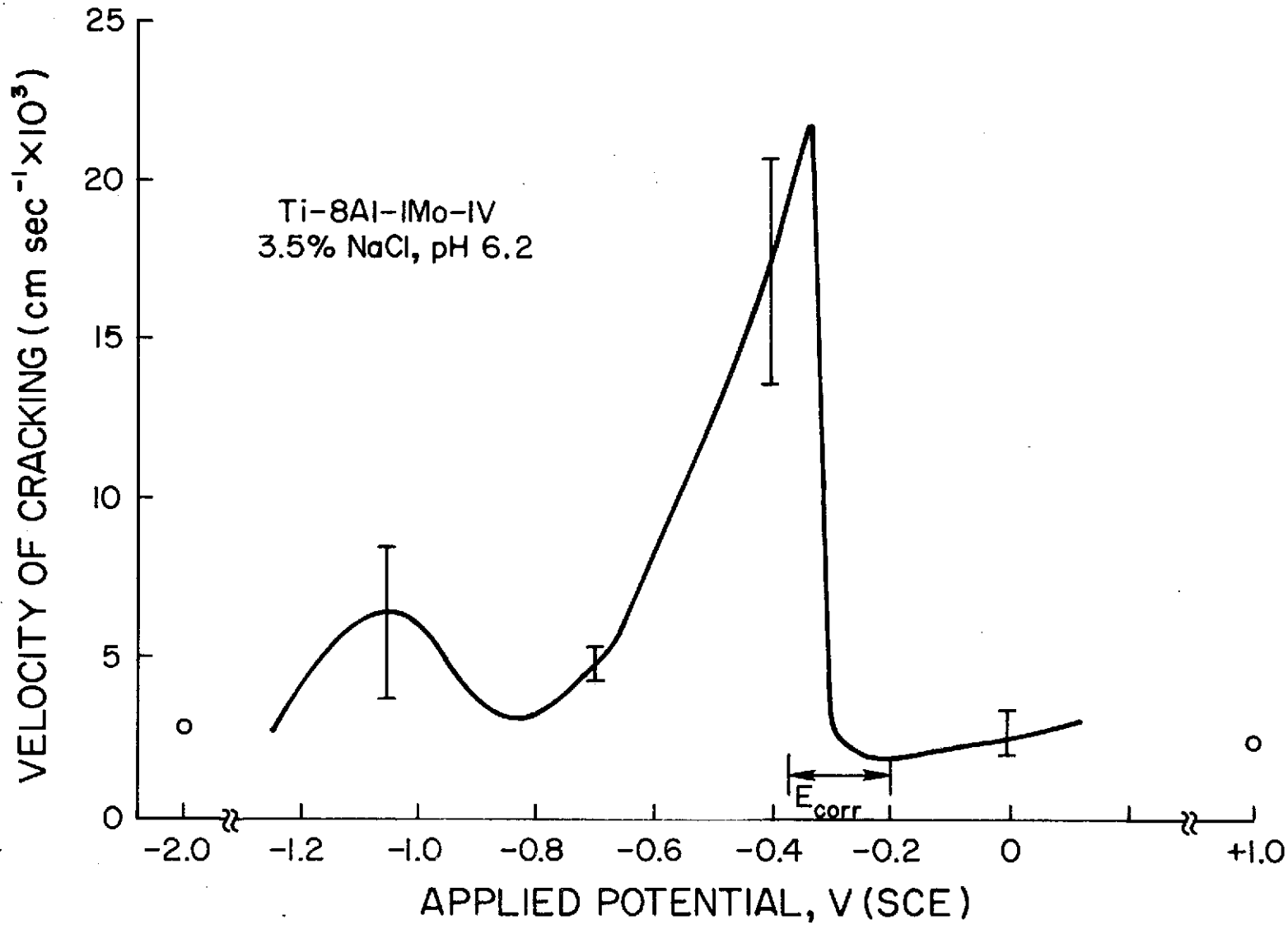

Fig. 1. The effect of applied potential on the velocity of cracking of Ti-8Al-1Mo-1V alloy in a neutral 3.5% NaCl solution (after Green and Sedricks[4]).

5-6 per cent aluminum and many investigators have related this to the formation of the ordered Ti_3Al phase.[11,12] R. A. Wood et al.[13,14] concluded that the size of the Ti_3Al particles was also important. They felt these particles cause a nonhomogeneous planar slip which leads to micro-void nucleation and coalescence by localized shear. The result is reduced fracture toughness and an enhanced chemical potential at the slip bands. They suggested the latter could contribute to sustain anodic dissolution. Yet, Owen et al.[15] have suggested that the role of Ti_3Al is to cause coplanar slip which they believe is a necessity for SCC. Lane et al.[16] reported that microstructures containing long coarse alpha were the most susceptible.

Heat treatment of the alloy is important to the resulting final microstructure and its susceptibility. The temperature range of 900-1500°F (482-816°C) was determined to give the most susceptibility due to Ti_3Al precipitation.[7] Also the alpha platelet size and its effect as determined by Lane[16] can be controlled by heat treatment.

May et al.[17] discussed the importance of surface layers to stress corrosion. He attributes the hydride surface layer as being most important in the susceptibility and refutes the oxide layer theory presented by other investigators.[12] Green and Sedricks[4] stated that their investigation showed that stress-corrosion cracking in Ti-Al alloys was confined to an environmental regime in which surface films are relatively thin. They theorized that the increased susceptibility with increased aluminum content was related to a thinner surface film formation, and that on even the most metallurgically susceptible alloys stress-corrosion cracking can be controlled by controlling those factors (i.e., pH and potential) which influence film formation.

There are many proposed mechanisms for stress corrosion in titanium alloys. These include stress sorption, brittle film failure, anodic dissolution, and hydrogen "embrittlement."

HYDROGEN IN TITANIUM

It has long been an accepted fact that hydrogen absorption into many metals causes "embrittlement" of one form or the other. Many authors have attempted to explain the role of hydrogen on the mechanical properties of metals and a good review of the subject is presented by Cotterill.[18] Some related hydrogen embrittlement of steel to the variables in the Griffith crack theory. For example, hydrogen adsorbed on the crack surface lowers the surface energy term; or the pressure of gaseous hydrogen in a microcrack adds to the total energy released by the system. A theory proposed by Morlett et al.[19] introduced the possibility of the embrittlement being due not only to hydrogen in voids, but also to hydrogen in the triaxial stress region created by the voids. The precise mechanism involving this hydrogen in solution at these regions was not explained.

In a recent article, C. D. Beachem,[20] suggested that hydrogen in steel may well act as a "plasticizer" rather than am embrittler. Thus, hydrogen aids whatever deformation process the state of stress at a crack tip may dictate. Observations showed that cracks propagated entirely by microscopic plastic flow at the crack tip during stress-corrosion cracking and hydrogen-assisted cracking. Microvoid coalescence, quasi-cleavage, or intergranular fracture were shown to occur depending on the stress intensity and the hydrogen concentration at the crack tip. The relationships of these are shown in Fig. 2. These findings are well accepted by those who contend that plastic instability in a material is a reality. This theory will be covered later in this presentation.

Unlike steel, which is classified as an endothermic occluder of hydrogen, titanium is an exothermic occluder. It is known to form a compound with titanium. Ideally the compound is TiH_2 but actually it is approximately $TiH_{1.5}$ - TiH_2.[21] Hydrogen in titanium has been associated with the embrittlement of the material. The embrittlement is divided into two categories depending upon the loading rate of the specimen. These are known as impact embrittlement and low-strain-rate embrittlement. Both types are believed to be due to the hydride phase precipitation. Williams[22] has related the impact embrittlement to hydrides formed on cooling to room temperature. If precipitation does not occur on cooling to room temperature a supersaturated condition exists and the action of strain can then cause hydride precipitation. This latter type is known as strain-induced hydride. Resistance to hydride precipitation has been associated with the solubility of hydrogen in the matrix and this solubility is apparently increased with certain alloy additions (i.e., aluminum). Boyd[21] made a thorough investigation of both the spontaneous and strain-induced hydrides formed in Ti-8-1-1. He believes that the effect of aluminum is to increase the activation energy of hydride nucleation, and that the strain-induced hydrides are nonequilibrium precipitates having lower activation energy for nucleation than the spontaneous hydrides. The general view of the mechanism of hydrogen embrittlement is one that the hydrides limit the amount of plastic deformation thus making the material less ductile. The effect is to cause a decrease in the reduction of area as the hydrogen concentration increases.

The data gathered on the mechanical properties of titanium and its alloy[23-25] show generally that the tensile and 0.2% offset yield strength increase with increased hydrogen concentration. However a point which is little emphasized is that--whether the 0.2% yeild strength decreases, stays relatively the same, or increases--the proportional limit generally decreases when hydrogen concentration increases.

A workable model based on the above theories of hydrogen embrittlement has been proposed to explain stress corrosion of titanium[26] and the conclusion that the model was basically correct for crack propagation was reached by Owen et al.[27] The model is based on the production of hydrogen which--during the corrosion of titanium--is adsorbed and

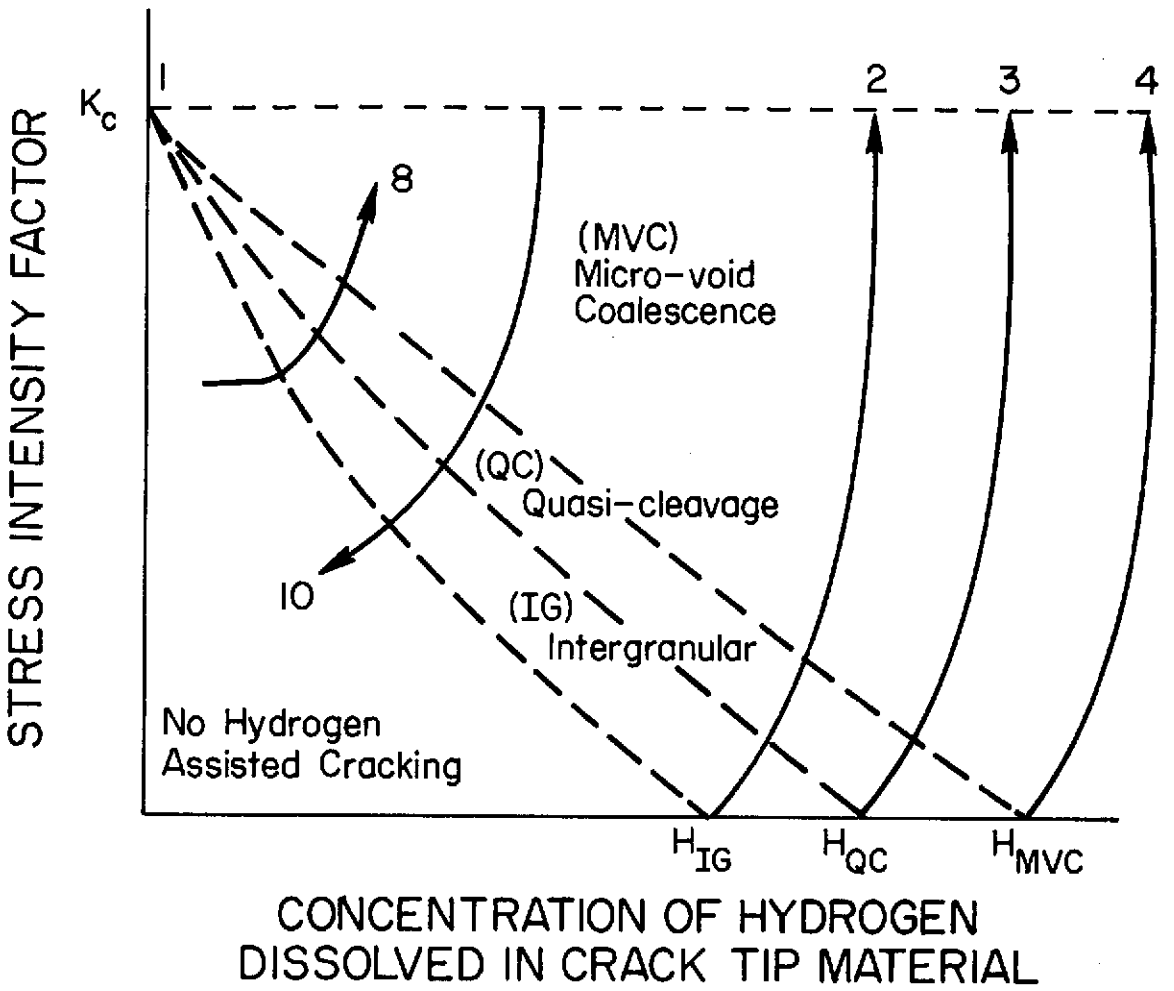

(1) No hydrogen
(2)
(3) Initiation in any of the three fracture
(4) modes depending on H_2 concentration
(8) Constant load with H_2 diffusing to crack tip causing shift to right
(10) Wedged specimens with decreasing stress intensity

Fig. 2. Interrelationship between stress intensity and dissolved hydrogen content (after Beachem[20]).

eventually absorbed into the lattice near the crack tip. It is partially based on Otsuka's[28] report that hydrogen is always absorbed when titanium is corroded in an acidic environment. The hydride responsible for stress-corrosion embrittlement is said to be the strain-induced (slow-strain rate) hydride. The hydride is thought to precipitate along active slip planes at the crack front. These hydrides are then thought to cause the slip planes to become inoperative and this in turn limits the plastic relaxation. Since slip is restricted, the plastic zone is thought to be very small--a condition promoting brittle fracture. Because of the velocity of the stress-corrosion crack this model depends on a discontinuous crack propagation where the crack can for a short distance outrun the hydrogen-containing lattice before crack blunting occurs. This condition is sometimes referred to as the "long-range effect."

The long-range effect has been examined by Spurrier and Scully[29] and found to be due to absorbed hydrogen which causes the initial fracture mode to penetrate the width of the grain and penetrate into adjacent grains if the misorientation is not too large. The long-range effect is due to a process referred to as low energy tearing (low energy relative to that required to tear dimples) and is said to be recognized fractographically as cleavage-like patterns, striations, and regions of planar slip. J. C. Scully has long been an advocate of hydrogen as the important element in the stress-corrosion cracking of titanium, as witnessed by some of his papers.[30-32] but this is the first paper that seemingly questions the role of hydrides. Reference is made to the possibility that hydrogen absorbed at the crack tip may result in striations caused by the interaction of plastic deformation on more than one slip system. This could then result in the production of cleavage-like river patterns originating from a plastic deformation process.

FRACTURE OF METALS

The language used by those engaged in fractography is confusing to say the least. Brittle fracture has been described by numerous surface fracture patterns whose distinction is rather ambiguous. These include cleavage, quasi-cleavage, river-pattern, transgranular striations, near classic cleavage, and nonclassic cleavage.[33] The distinction seems to be how much or how little plastic deformation has occurred. Recent work has indicated that plasticity is an important feature of practically all fracture, even in the field of stress corrosion. Colangelo and Ferguson[34] showed that the path of the primary stress corrosion crack in a high-strength steel (4340) followed the shear bands within the plastic zone at the crack tip.

The two basic modes of fracture are categorized as (1) pore formation and coalescence, and (2) plastic instabilities in the direction of pure shear.

Pore formation--sometimes known as cavitation--is nucleated at some discontinuity in the matrix (inclusions, precipitates, grain boundaries, etc.). These pores then increase by further plastic deformation and when the loading is halted the pores stop growing. This is the concept of pure ductile fracture. As the load is increased the ligaments between the pores reduce in size like tiny tensile specimens until rupture or 100% reduction occurs. The stress state of the system is an important factor in the final shape of these pores, as has been shown by the work performed by Beachem.[35]

Plastic instability in pure shear directions, defined as the localization of plastic flow leading to highly concentrated strain, has been the subject of intensive studies by Spretnak, one of the authors of this paper. Clear evidence of this phenomenon leading to fracture has been given by Hayden and Floreen.[36] This phenomenon is not to be confused with the geometric instability which is the typical necking experienced in tensile tests. A comparison of the mathematical models of these instabilities is presented by Chakrabarti.[37] The localization defined as plastic instability has been shown[38-40] to take place along characteristics determined by continuum plasticity theories. These are directions of pure shear (zero extensional strain) and in plane strain conditions (maximum shear stress directions). This instability or discontinuity in tangential velocity is based on the material reaching the ideally plastic state in which the stress cannot be raised above the flow stress. Mathematically the ideal plastic state occurs when

$$d\sigma/d\epsilon = 0 \quad \text{and} \quad d\sigma_{ij}d\epsilon_{ij} = 0 .$$

The latter expression shows that over a finite strain value no work is accomplished. The equation predicting this instability phenomenon can be shown to be

$$d\sigma = \left(\frac{\partial\sigma}{\partial\epsilon}\right)d\epsilon + \left(\frac{\partial\sigma}{\partial\dot{\epsilon}}\right)d\dot{\epsilon} + \left(\frac{\partial\sigma}{\partial T}\right)dT \leq 0 .$$

Thus, the condition is dependent on the strain, strain rate, and change of stress by adiabatic heating.

Plastic instability failures normally occur as three distinct types. The first type occurs as highly localized plastic flow with the thickness of the instability band being smaller than any second-phase particles in the matrix (the fracture surface would be very flat and generally particle free). This type is referred to in the literature as a quasi-cleavage fracture, and is supported by Chang[41] who observed plastically deformed metal just below the quasi-cleavage fracture surface. Thus, the fracture was not caused by metal reaching its theoretical cohesive strength and cleaving.

When the plane of instability flow is thicker than second-phase particles there is a tendency toward pore formation at those particles within the plane of instability and coalescence of these pores occurs. This is designated as the second type of instability controlled flow.

The third type may not actually be instability controlled although it may be instability flow limiting. It occurs when diffuse deformation produces pores which are then connected by instability flow. Thus, the instability limits the total deformation possible when 100% reduction of ligaments between pores has occurred.

Since plain strain conditions can exist at notches and flaws in material, the localization of plastic flow is believed to be basic for the development of crack instability. Thus, fracture of the material occurs by either localization (for those materials having low resistance to plastic instability) or by decohesion due to pore formation and coalescence (for those materials having high resistance to plastic instability and which are interrupted by this latter process before localization of flow can occur). The instability condition is thus basic to the understanding of "brittle" fracture where brittle fracture is defined as unstable crack propagation. It is based on the exhaustion of strain hardening and the obtaining of a state of dynamic ideal plasticity in a very localized region. This plasticized state and its relationship to fracture in metals is described by Spretnak.[42] It is an important condition in both ductile and so-called brittle materials. And since stress-corrosion cracking, except for those conditions where total reliance upon anodic dissolution has been proven, adheres to the fundamental fracture modes these fracture modes are important to the understanding of stress-corrosion cracking.

Recht[43] postulated that titanium and its alloys should be particularly susceptible to localized plastic shear and showed this in his machining experiments. Work by Ernst and Spretnak[38] showed that the susceptibility of titanium alloys was between those AISI 4340 alloy steel having 178 ksi tensile strength and AISI 4340 having 217 ksi tensile strength. They also showed that the strength of the instability was very great compared to AISI 4340. In other words fracture occurred immediately after the instability appeared. Their work further demonstrated that instability formation is favored by high strain rates. Chakrabarti[37] showed that the lower the strain-hardening capacity and the strain-rate sensitivity of the material (4340) the lower the strain to the onset of shearing instability and the strain to failure. Because of the high strain-hardening exponent for titanium it is expected that strains to the onset of instability and failure will be relatively high.

EXPERIMENTAL PROCEDURES

Two titanium alloys, supplied by Reactive Metals, Inc., were used for this study. Chemical analyses of the alloys are given in Table I. Since the alloys were treated in different manners with respect to specimen design and preparation and since they behaved differently experimentally, the two alloys will be handled separately in the description of this study.

Table I. Chemical Analysis of As-Received Titanium Sheet

	Ti-5Al-2.5Sn (wt %)	Ti-8Al-1Mo-1V (wt %)
Aluminum	5.0	7.85
Tin	2.5	--
Iron	0.04	0.13
Oxygen	0.091	0.08
Nitrogen	0.012	0.008
Carbon	0.01	0.02
Vanadium	0.02	1.05
Molybdenum	< 0.01	1.1
Manganese	0.03	--
Copper	< 0.01	--
Hydrogen	--	0.01

ALLOY Ti-5Al-2.5Sn

The alloy used for the initial tests was Ti-5Al-2.5Sn of the ELI (extra-low interstitial) designation. Extra low interstitial was selected in order to obtain an all alpha microstructure (commercial Ti-5Al-2.5Sn contains a small amount of beta phase).

The material was originally stocked as 0.2 inch (5.08 mm) plate. It was then hot-rolled by RMI and "conditioned" (etched) to a thickness of 0.76 mm. The individual specimens were then wet ground in a fixture to 0.66 mm through 600 grit silicon carbide metallographic paper. Specimens were cut from the sheet such that the longitudinal axis of the tensile specimen was parallel to the rolling direction of the sheet. Final grinding was also performed such that the final cutting direction was parallel to the longitudinal axis. Thus, no transverse marks were found on the specimens. The specimens were milled to the dimensions shown in Fig. 3 to provide a width-to-thickness ratio of 25:1 (in bending this has been shown to be the critical ratio necessary for a plane

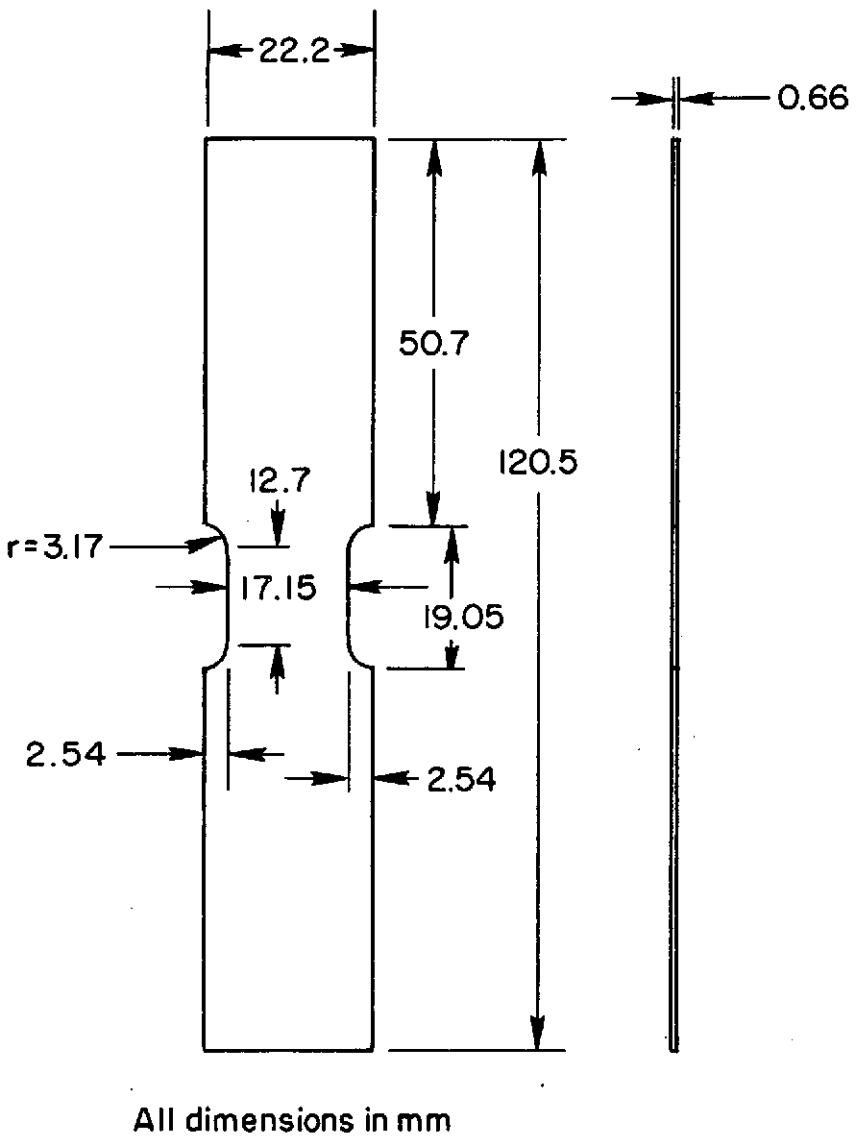

Fig. 3. Sheet tensile specimen for Ti-5Al-2.5Sn

strain state of stress). Also, work by Chakarbarti[37] has shown that curves relating strain to onset of instability and to failure started to flatten out at width/thickness ratios greater than about 25:1.

This experiment was concerned with finding the effect of hydrogen concentration on plastic instability formations and was designed such that pore formation and its interruption of this instability phenomenon would not occur. Thus, phase interfaces like α-β, where pore formation is enhanced, were eliminated by using the ELI material. Hydrogen was charged at high temperature as a gas to obtain hydrogen homogeneity.

Initially all specimens were vacuum annealed to obtain a low reference hydrogen level. The vacuum anneal cycle was $3\frac{1}{2}$-4 hr at 810°C followed by a furnace cool in vacuum. The vacuum obtained was 0.8-1.0 x 10^{-7} mmHg. The level of hydrogen obtained after this treatment was checked by Leco Technical Service Laboratory, St. Joseph, Michigan. Analysis showed an average hydrogen content of 10.5 ppm. This compares well with values obtained by others using a similar thermal treatment.[44]

The hydrogenation procedures were similar to those used by Trzeciak.[45] A diagram of the equipment used in the present study is shown in Fig. 4. A very-slow-leak valve allowed maximum efficiency in the cold trap between the gas source and the specimens and a capsule whose volume had been premeasured was filled to a specific pressure depending on the amount of gas which was desired to diffuse into the titanium sample. (The appendix contains a typical calculation used to give a particular concentration of hydrogen.) The capsule was then sealed off and heat treated in a box furnace. Heat treatment was 820°C for 20 minutes followed by a furnace cool to 680°C for a total furnace time of $2\frac{1}{2}$ hours. The sample was rapidly cooled from 680°C.

This charging procedure is based on the fact that titanium is a very good "getter" of hydrogen and will quickly absorb the gas available in the capsule (to the equilibrium vapor pressure of approximately 10^{-2} mmHg at room temperature). The concentrations of hydrogen used in this study were such that at the homogenizing temperature the hydride was not stable, as shown in work by Lenning.[44] Thus, except for the highest concentrations, the hydrogen absorption depended on a titanium-hydrogen interaction but not on hydride formation. Lenning[44] showed that hydrogen concentration throughout a specimen charged in this manner was uniform.

Predetermined levels of hydrogen were 10, 80, 150, and 500 ppm. The actual content was determined using a hydrogen analysing apparatus--based on a gas chromatograph sensing system--developed in this laboratory. The operation of this equipment is described by Gloz.[46] A brief summary (below) of the apparatus will give the reader an appreciation for the potential of this procedure.

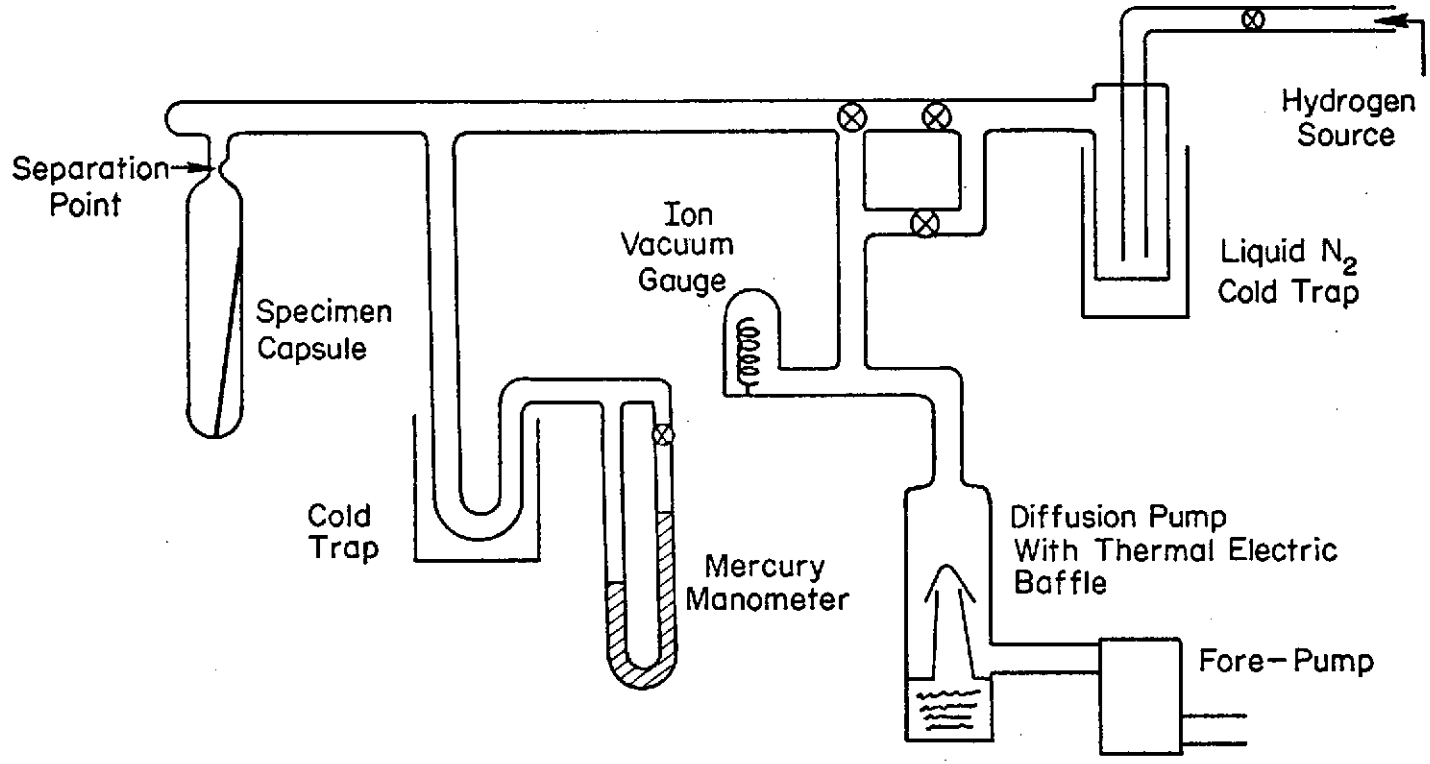

Fig. 4. Diagram of hydrogenating system

Basically the system consists of an induction coil furnace to heat a small pre-weighed specimen of the metal and thus drive off the hydrogen. The specimen is located in a tubing system which has been evacuated. The same diffusion pump used for evacuation is used to pump the hydrogen, driven off by heating of the specimen, into a particular area of the system. This hydrogen is then transferred by a mercury pump to a collection station previously purged with nitrogen where volumes can be measured. A syringe is then used to transfer a given amount of the hydrogen and nitrogen gas mixture to the gas chromatograph where the hydrogen concentration is graphically plotted. A hydrogen gas standard is used to check the gas chromatograph, and National Bureau of Standards Ti-H samples are used to check the collecting system during any set of runs. As an example of the accuracy of the system, the samples reported by Leco to contain 10.5 ppm hydrogen were also analyzed with this gas chromatograph method and found to contain 9.7 ppm hydrogen. Table II gives results of further analyses performed on charged specimens.

Table II. Hydrogen Concentration of Selected Specimens

Specimen	Calculated Hydrogen (ppm)	Actual Measured Hydrogen (ppm)
1 - Test Strip (vacuum annealed)	10	9.5
2 - Tensile Specimen (vacuum annealed)	10	12.5
3 - Test Strip (hydrogen charged)	125	123
4 - Test Strip (hydrogen charged)	250	265
5 - Tensile Specimen (hydrogen charged)	150	154

After charging the specimens were marked (printed) with a grid pattern. Thus, by following the grid distortion, the strains at a given load could be calculated. The grid printing procedure was outlined in the work by Chakabarti[37] and a modified reproduction is given below.

(1) The printing surface is thoroughly cleaned and degreased using acetone.

(2) A thin uniform layer of coating solution is applied to the surface to be printed by wiping with a soft, solution-saturated tissue. (The coating solution consists of a 50-50 mixture of Kodak Photo Resist and Kodak Photo Resist Thinner.)

(3) The coating is allowed to air dry (in the dark) for at least 45 minutes.

(4) The coated specimen is then exposed to ultraviolet light for 3 to $3\frac{1}{2}$ minutes. (It is very important that good contact exist between the grid negative and the sample--weights may be necessary to optimize the contact.) Another important step is to keep the lamps as cool as possible. Heat locally was extremely concentrated and a fan was used for cooling.

(5) The specimen is then dipped in Kodak Photo Resist Developer for 2 minutes followed by Kodak Photo Resist Black Dye for 15 seconds.

(6) The specimen is then rinsed in slowly running water for about 5 minutes.

(7) The specimen is then air or force dried at 90°C for about 5 minutes.

The grid pattern produced is very distinct and the particular negative used in this experiment gave square grids of 20 lines/inch over the gage length of the specimen. The prepared specimens were then stored in liquid nitrogen until the time they were tested.

Specimens were tested with an Instron tensile testing machine at room temperature using a crosshead speed of 0.2 cm/minute. In the gage length used this produced a strain rate of 0.1575 min^{-1}. The specimens were mounted in grips and alignment was kept as perfect as possible. Poor alignment would have been visible during the testing since deformation bands were visible on the specimens. Work prior to the actual testing, using strain gages mounted to the sheet specimens, showed that all gages were reading within 1% of each other and thus bending was minimal.

The load was recorded on a X-Y plotter with one parameter being the time function. Distortion of the grids with load was recorded by a 35 mm Nikon camera mounted a small distance from the specimen surface. The corresponding load was marked on the X-Y chart each time the camera shutter was released.

Calculations of true stress versus true strain were made using measurements taken from the grid deformation. (The film negatives were enlarged approximately ten times, which resulted in an actual grid size

enlargement of about 7X.) Using spring-loaded dividers and a scale divided into increments of 1/100 inch, the length and width measurements of the grid were obtained. From these true strain could be obtained, since it is the natural logarithm of the instantaneous length divided by the original length ($\epsilon = \ell n$ L/Lo).

This relationship is true up to the point of necking but at that point accuracy decreases. The amount of error is small if the necking is small and the only way of obtaining a true value would be to use $\epsilon = \ell n$ Ao/A. This would mean that a way of measuring instantaneous thickness as well as width would be needed. For the Ti-5Al-2.5Sn alloy the necking was greater than for the Ti-8Al-1Mo-1V alloy. As will be shown in the Discussion, the latter alloy had strain values that agreed well with those based on the final area.

From the experiments it was intended that strain parameters measured as above could be related to instability formation or load disruption, and could then be compared at various hydrogen levels.

ALLOY Ti-8Al-1Mo-1V

Figure 5 shows the tensile specimens used for the Ti-8Al-1Mo-1V alloy. This alloy was of a higher strength than the former one and specimens were designed to give more constraint with a width-to-thickness ratio of 32:1. The composition of the alloy is given in Table I. A small percentage of β phase was present as islands in the α phase. The specimens were prepared similarly to the Ti-5Al-2.5Sn except for the thermal treatment which consisted of a vacuum anneal at 810°C for 4 hours and furnace cool. Specimen capsules were backfilled with hydrogen to obtain levels of 10, 80, and 150 ppm. These levels were chosen because work performed by J. D. Boyd[21] had shown that 200 ppm or more of hydrogen would result in strain-induced hydrogen precipitation. The particular interest in the present study was the effect of interstitial hydrogen and not hydride.

Following hydrogen backfilling of the capsules the specimens were heated at 810°C for two additional hours. The specimens were next cooled to 650°C, held for one hour, and then part of them were fast-quenched while remaining specimens were furnace-cooled to 600°C for 24 hours and 550°C for 24 hours to duplicate heat treatments used by Boyd et al.[47] This latter treatment was used in order to obtain specimens with the α_2 compound, Ti_3Al. It has been shown that alloys containing this compound are more sensitive to stress corrosion cracking because of the embrittling effect of the compound. The hardness of the specimens was checked to verify compound formation. As in the previous procedures the 10 ppm samples were encapsulated and backfilled with argon so that the thermal cycle on these specimens would be identical to their hydrogen charged counterparts.

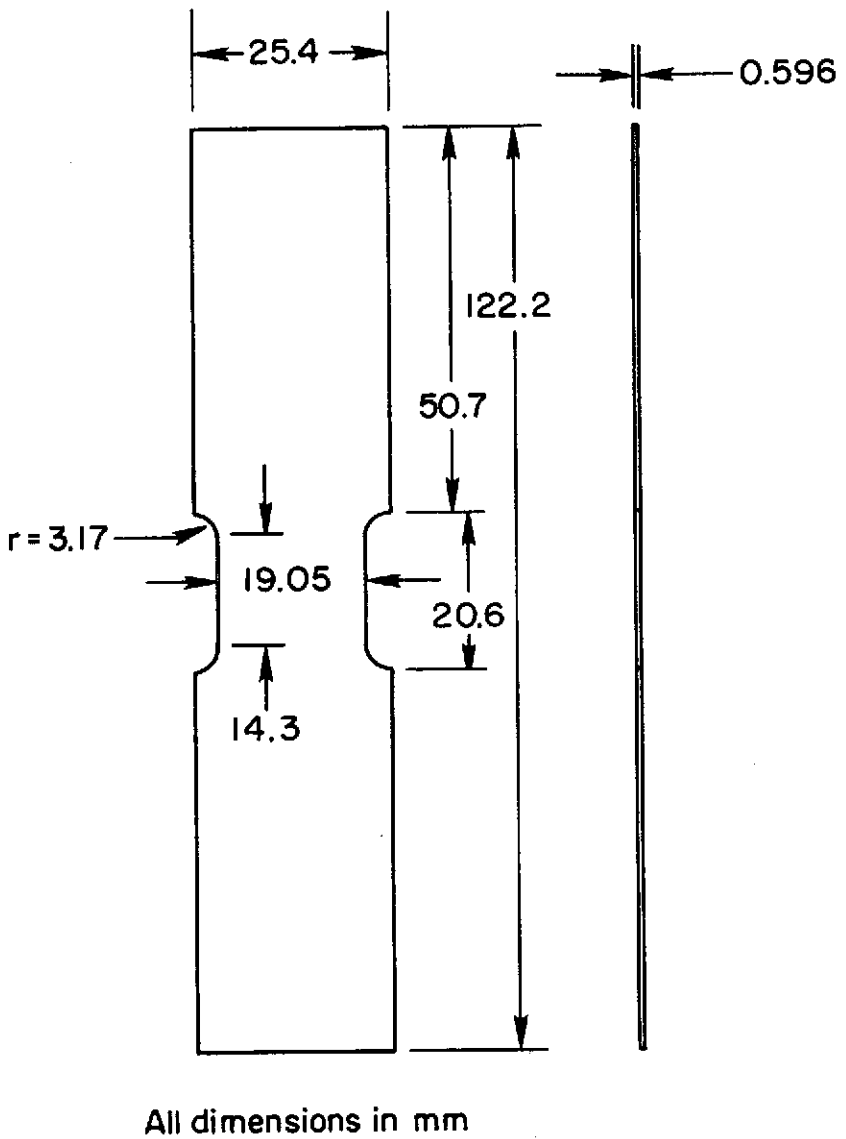

Fig. 5. Sheet tensile specimen for Ti-8Al-1Mo-1V

The grid pattern was placed on the Ti-8Al-1Mo-1V alloy specimens using a different technique than that for the Ti-5Al-2.5Sn specimens. A ballpoint pen was attached to a vernier height gage having scale increments of 0.025 inch (0.634 mm). The specimens were mounted to precision-ground blocks and the grid lines were drawn on the specimens one line at a time.

RESULTS

Ti-5Al-2.5Sn ALLOY

The mechanical properties of the vacuum-annealed Ti-5Al-2.5Sn specimens were 667 MN/m^2 (96,000 psi) 0.2% offset yield strength, 715 MN/m^2 (103,000 psi) tensile strength, and 24% elongation. These values compared well with the minimum values specified in company brochures which were 695 MN/m^2 tensile strength, 626 MN/m^2 yield strength, and 10% elongation. Figure 6 shows the grain structure obtained, the grain size being 290 x 10^{-4} mm. Table III contains the tabulated results of the 0.2 cm/min crosshead speed test. The instantaneous area was calculated assuming the volume remains constant and thus

$$l'w't' = l_o w_o t_o$$

and

$$t' = \frac{l_o w_o t_o}{l'w'} ,$$

where t' is the instantaneous thickness.

The instantaneous area (A_i) is then equal to t' x w'.

Figures 7 and 8 show the results of plotting true stress versus true strain. These results illustrate that the true stress reached a maximum value and did so at a strain greater than the maximum load point. Chakrabarti[37] showed this maximum true stress value to be the onset of the instability meeting the condition

$$d\sigma = \left(\frac{\partial\sigma}{\partial\epsilon}\right)d\epsilon + \left(\frac{\partial\sigma}{\partial\dot{\epsilon}}\right)d\dot{\epsilon} + \left(\frac{\partial\sigma}{\partial T}\right)dT \leq 0 .$$

Ernst[48] showed that the plastic instability in titanium alloys under a torsional state of stress was very strong. In other words, the strain at onset of instability minus the strain at failure ($\epsilon_{ins} - \epsilon_f$) was very small. This is observed to be true in the present experiments. From the graphs it can be seen that failure occurred very soon after the true stress maximum. Synthesis of the data obtained from the graphs is shown in Table IV. No values are given for disruption strain in the 10 ppm hydrogen sample because there was no real disruption stage. The crack appeared at the edge and grew slowly along the deformation band; most of the growth was in this stable manner. Therefore, at the given strain rate, instability fracture in the specimen was not manifested.

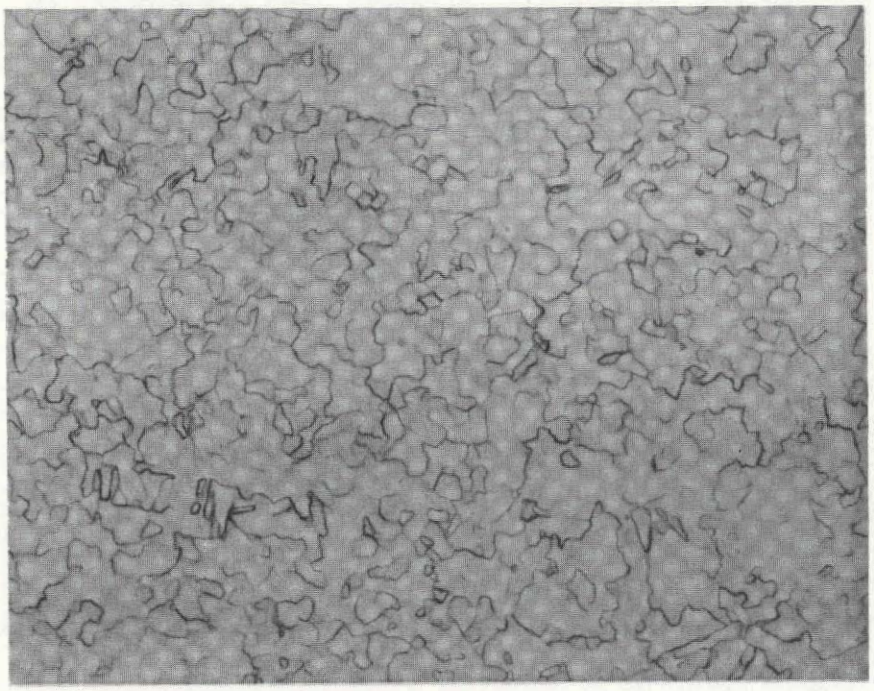

Fig. 6 - Fine grain structure on Ti-5Al-2.5Sn sheet containing 10 ppm hydrogen 250X

Table III. Ti-5Al-2.5Sn Alloy: True Stress and True Strain Data for a Strain Rate of 0.1575 Min^{-1}

Photo	Measured Width (in.)	Measured Length (in.)	True Strain (ℓn L/Lo)	Instantaneous Area $(mm)^2$	Load (kg)	Load (lb)	True Stress (ksi)	True Stress (MN/m^2)
10 ppm hydrogen; original measured, width-3.30 in., length-4.05 in. (Photo 3)								
5	3.33	4.02	.009	11.21	740	1630	93.8	651.9
8	3.37	3.96	.021	11.10	802	1765	102.7	713.8
12	3.49	3.84	.055	10.70	820	1805	109.0	757.6
14	3.57	3.74	.079	10.47	821	1807	111.2	772.8
16	3.71	3.57	.117	10.08	808	1779	113.8	790.9
18	3.82	3.48	.146	9.77	790	1740	114.9	798.6
19	3.88	3.38	.161	9.64	780	1717	114.8	797.9
20	3.92	3.35	.172	9.53	770	1695	114.8	797.9
21	3.95	3.29	.180	9.46	752	1655	113.0	785.3
22*	3.98	3.27	.187		690	1520		
23	4.02	3.23	.197					
24	4.09	3.15	.215					
25	4.31	3.02	.267					
80 ppm hydrogen; original measured, width-5.72 in., length-4.64 in. (Photo 1)								
2	5.71	4.71	.015	10.74	826	1817.2	109.3	760
4	5.63	4.82	.038	10.49	852	1874.4	115.3	801
6	5.49	4.92	.059	10.30	860	1892.0	118.7	825
7	5.42	4.97	.069	10.19	860	1892.0	119.8	833
9	5.25	5.12	.098	10.02	860	1892.0	122.0	848
10	5.17	5.19	.112	9.77	852	1874.4	124.0	862
11	5.10	5.24	.121	9.67	843	1854.6	123.9	861
13	4.89	5.42	.155	9.34	832	1830.4	126.5	879
14	4.74	5.53	.175	9.15	812	1786.4	126.1	876
15	4.66	5.60	.188	9.06	800	1760.0	125.6	873
16	4.58	5.69	.204	8.89	787	1731.4	125.7	874
17	4.49	5.75	.214	8.82	780	1716.0	125.7	874
18	4.37	5.86	.233	8.63	762	1676.4	125.4	872
19	4.27	5.94	.247	8.53	749	1647.8	124.7	867
150 ppm hydrogen; original measured, width-5.74 in., length-4.67 in. (Photo 21)								
22	5.72	4.73	.013	11.42	875	1922.8	108.6	755
23	5.65	4.79	.025	11.28	895	1969.0	112.8	784
25	5.38	4.93	.054	10.97	903	1986.6	117.0	813
26	5.26	5.04	.076	10.73	903	1986.6	119.5	831
27	5.13	5.15	.098	10.49	897	1973.4	121.5	844
29	4.98	5.29	.125	10.20	882	1940.4	122.8	853
30	4.85	5.39	.143	10.02	870	1914.0	123.4	858
31	4.74	5.49	.162	9.85	855	1881.0	123.5	858
32	4.65	5.57	.176	9.72	845	1859.0	123.7	860
33	4.53	5.67	.194	9.53	830	1826.0	123.9	861
34	4.44	5.75	.208	9.38	820	1804.0	124.2	863
35	4.25	5.91	.235	9.13	787	1731.4	122.4	851
36			.247				121.1	842
500 ppm hydrogen; original measured, width-4.99 in., length-4.05 in. (Photo 1)								
2	4.92	4.05		11.32	870	1915	109.1	758.2
3	4.89	4.06	.002	11.27	932	2051	117.5	816.6
4	4.84	4.13	.019	11.12	967	2128	123.6	859.0
5	4.78	4.19	.034	10.92	971	2138	126.2	877.1
6	4.73	4.24	.046	10.82	975	2145	128.1	890.3
7	4.67	4.28	.055	10.71	976	2148	129.6	900.7
8	4.58	4.38	.078	10.47	977	2150	132.5	920.9
9	4.47	4.47	.099	10.24	978	2152	135.7	943.1
10	4.37	4.59	.125	9.97	977	2150	139.2	967.7

*Appearance of first crack

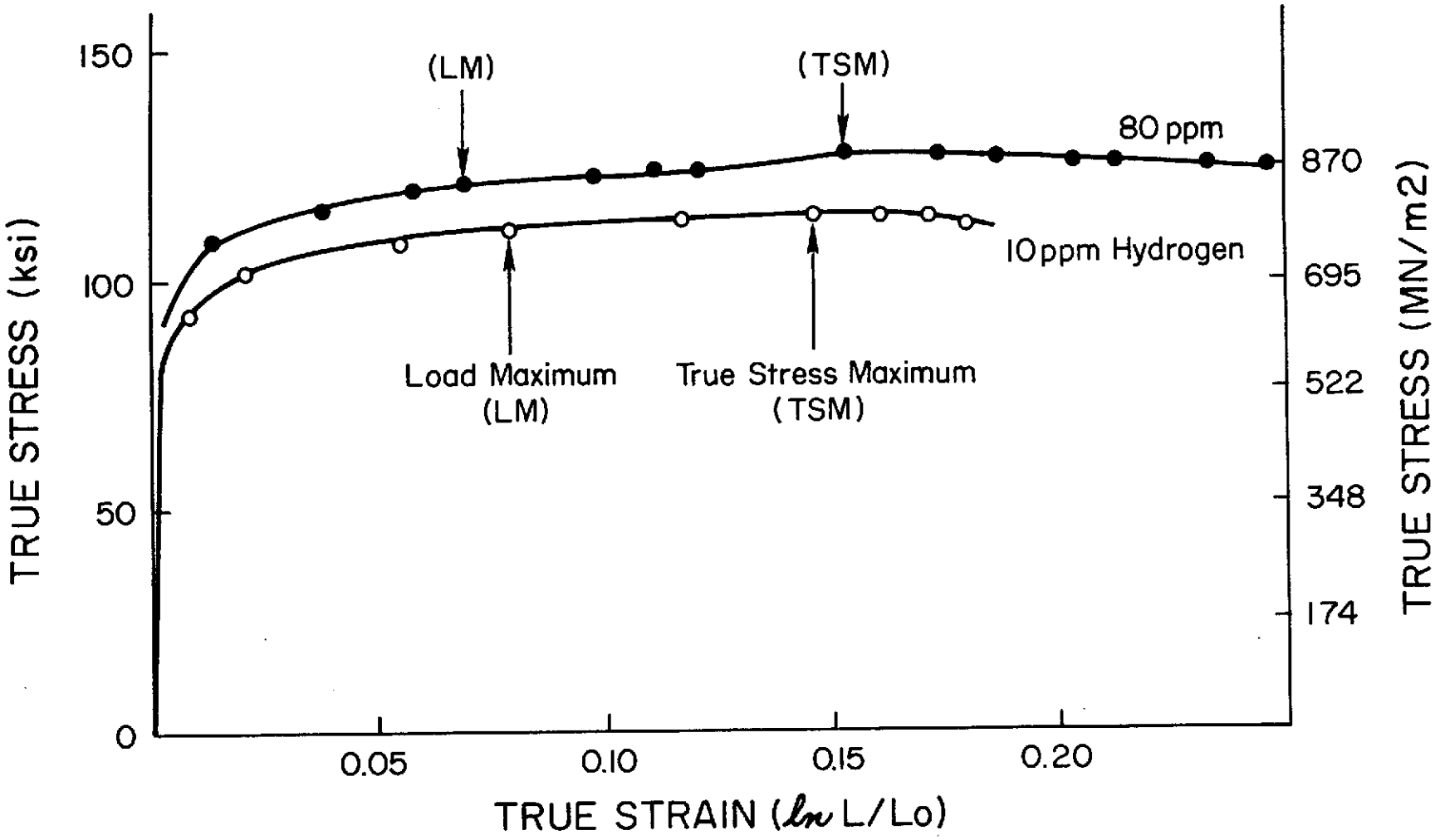

Fig. 7. True stress vs true strain for Ti-5Al-2.5Sn with strain rate 0.1575 min^{-1}

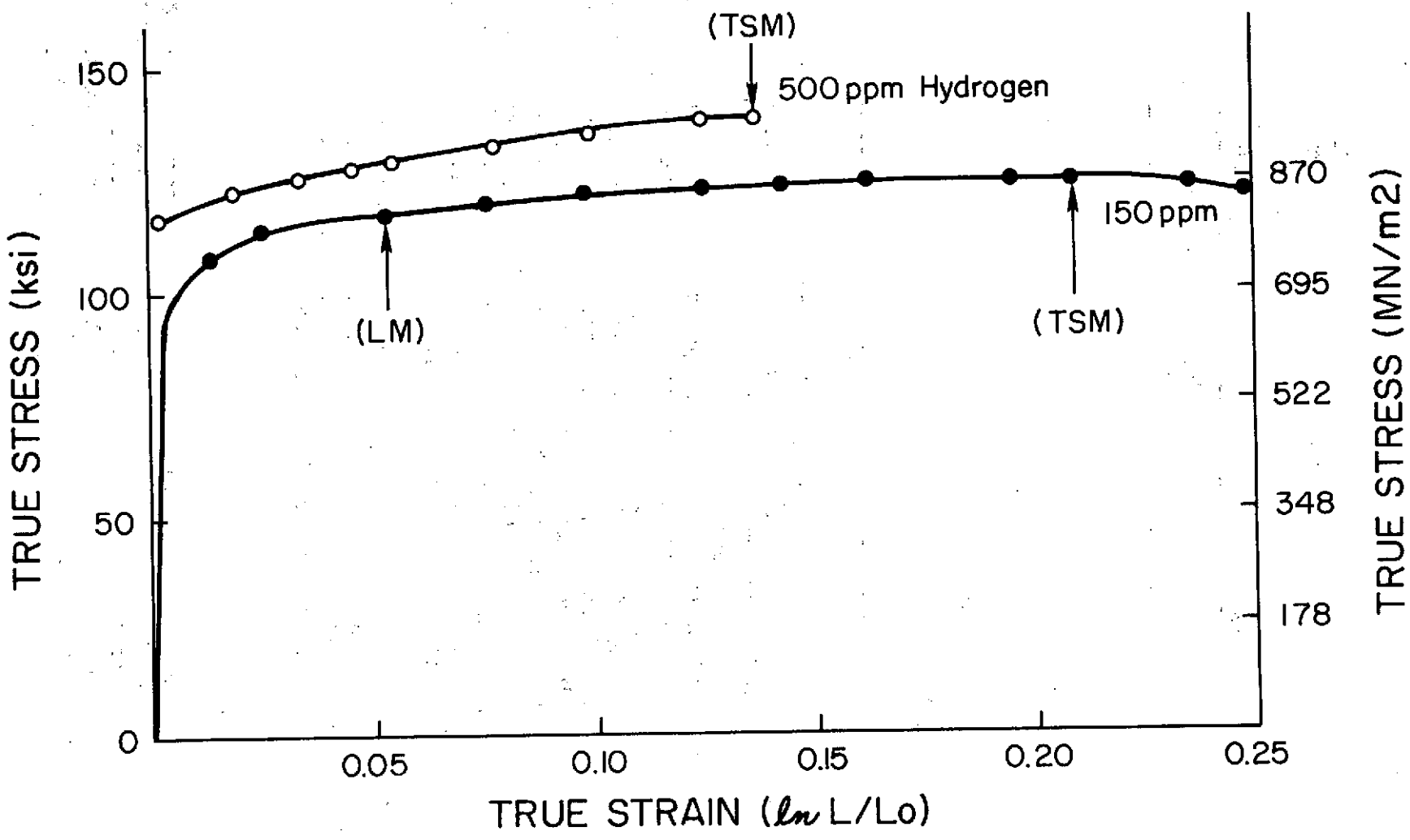

Fig. 8. True stress vs true strain for Ti-5Al-2.5Sn with strain rate 0.1575 min^{-1}

Table IV. Strain Parameters for Ti-5Al-2.5Sn Alloy as Affected by Hydrogen Concentration

Crosshead Speed 0.2 cm/min; Strain Rate 0.1575 min^{-1}

	Hydrogen Concentration (ppm)			
	10	80	150	500
Strain at $d\sigma = 0$	.146	.155	.208	.137
Strain at Disruption	--	.247	.247	.137
True Stress at Disruption (MN/m^2)		864	843	968
(ksi)		124.1	121.1	139.5

Of particular concern to this study was the effect of the interstitial hydrogen. Lenning[49] had shown that the hydrogen solubility in a Ti-5Al alloy was approximately 200 to 300 ppm. The data in Figs. 7 and 8 of the present work indicate that between 150 and 500 ppm hydrogen were sufficient to cause spontaneous hydride precipitation. The photomicrograph (Fig. 9) shows hydride precipitate in a sample containing 500 ppm hydrogen. The hydride is mostly grain boundary oriented, although a few hydride spikes can be seen in the grains. It would be expected that as the alloy content increased or as the supersaturation of hydrogen increased, more and more of the hydrides would precipitate on particular habit planes in the titanium crystal. These planes have been indexed by a number of investigators.[21-27] This spontaneous hydride precipitation resulted in a definite decrease in the ductility of the material. The strain to failure was determined to be lower than those of the less concentrated samples.

Examination of the fracture patterns of the specimens showed a variety of results. Figure 10 shows a sample of one of these. Although it appeared as though some of the specimens initiated fracture from the edge, initiation occurred primarily in the center.

Ti-8Al-1Mo-1V ALLOY

The Ti-8Al-1Mo-1V specimens had a tensile strength of 1012 MN/m^2 and a yield strength of 963 MN/m^2. Figure 11 shows the grain structure of the specimens after vacuum annealing. The α grain size was measured to be 145 x 10^{-4} mm. As can be seen, islands of β phase exist at the α grain boundaries. Table V gives the deformation measurements taken on some of the specimens tested. As can be seen from Figs. 12 and 13

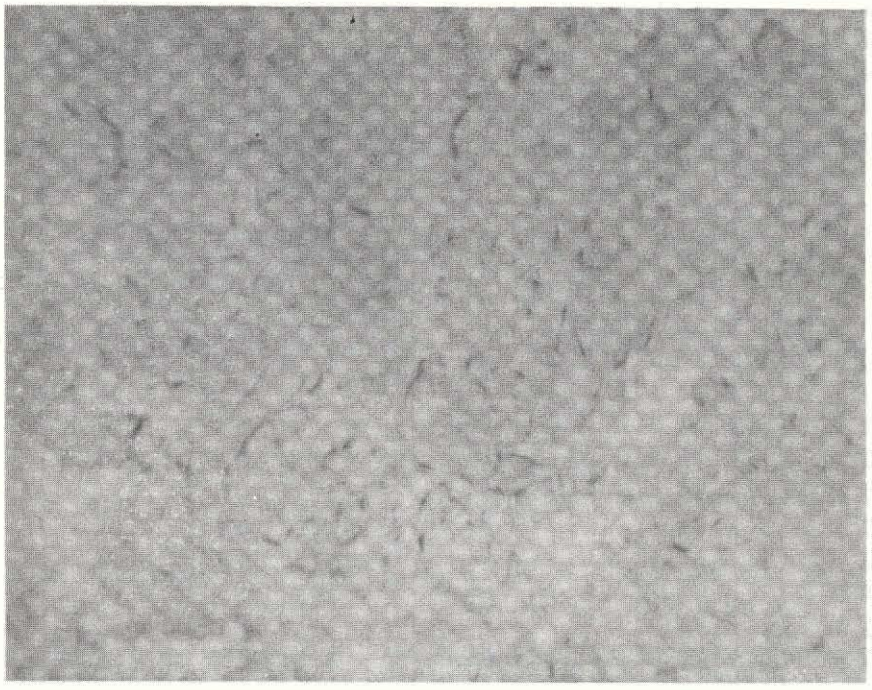

Fig. 9 - Hydrides present in the Ti-5Al-2.5Sn alloy containing 500 ppm hydrogen 500X

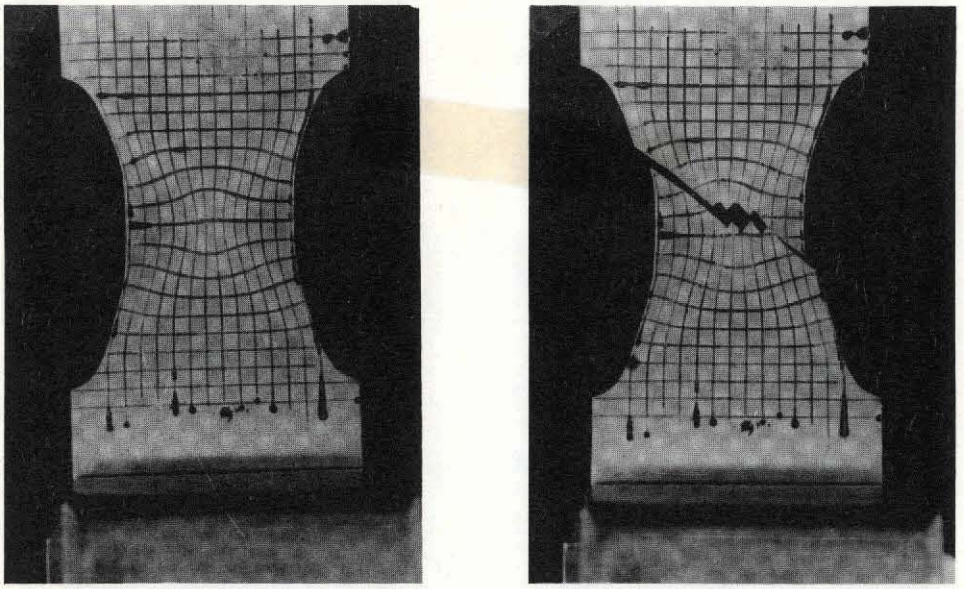

Fig. 10 - Fracture events for Ti-5Al-2.5Sn with 80 ppm hydrogen at 0.1575 min^{-1} strain rate

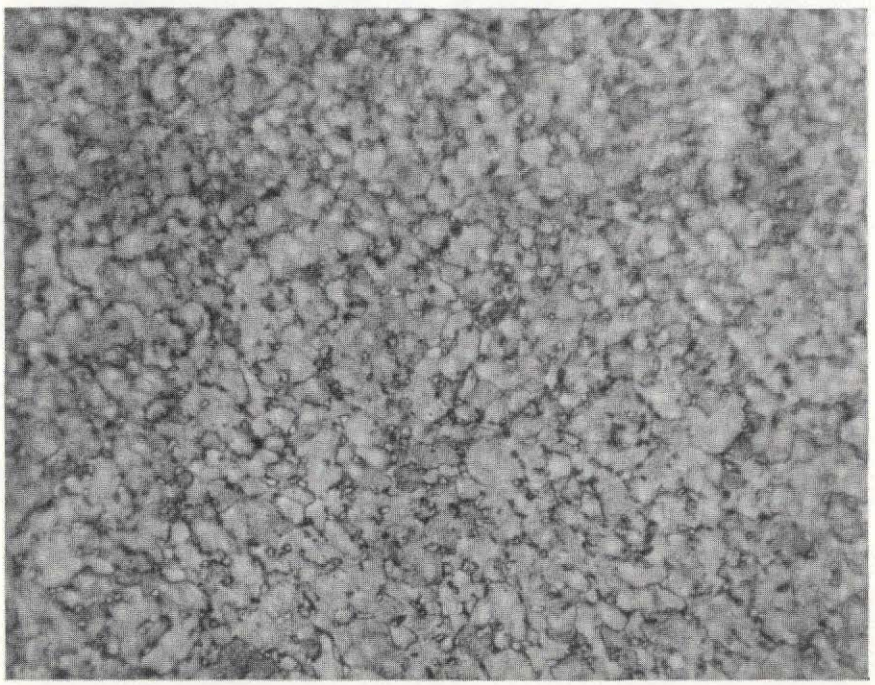

Fig. 11 - Vacuum annealed Ti-8Al-1Mo-1V alloy showing fine α grain size with islands of β phase 500X

Table V. Ti-8Al-1Mo-1V Alloy: True Stress and True Strain Data for a Strain Rate of 0.140 Min^{-1}

Photo	Measured Width (in.)	Measured Length (in.)	True Strain (ln L/Lo)	Instantaneous Area $(mm)^2$	Load (kg)	Load (lb)	True Stress (MN/m^2)	True Stress (ksi)
80 ppm hydrogen; original measured, width-5.79 in., length-4.18 in. (Photo 14)								
16	5.71	4.33	.035	10.75	1099	2418	1008.4	145.1
17	5.64	4.43	.058	10.49	1114	2451	1047.4	150.7
18	5.58	4.52	.078	10.31	1124	2473	1075.9	154.8
19	5.52	4.57	.089	10.19	1129	2484	1092.5	157.2
20	5.49	4.62	.100	10.07	1129	2484	1105.7	159.1
21	5.45	4.65	.106	10.00	1130	2486	1114.8	160.4
22	5.40	4.72	.121	9.86	1134	2495	1134.9	163.2
24	5.37	4.77	.132	9.75	1136	2499	1148.6	165.3
25	5.22	4.97	.173	9.36	1136	2499	1196.8	172.2
26	5.19	5.01	.181	9.28	1134	2495	1205.1	173.4
27	5.13	5.05	.189	9.22	1129	2484	1207.9	173.8
28	5.10	5.10	.199	9.13	1114	2451	1203.7	173.2
29	5.06	5.14	.207	9.06	1106	2433	1203.7	173.2
150 ppm hydrogen; original measured, width-5.77 in., length-4.23 in. (Photo 1)								
3	5.63	4.40	.039	10.92	1144	2517	1034.2	148.8
4	5.56	4.52	.066	10.65	1158	2548	1073.1	154.4
5	5.51	4.58	.079	10.50	1160	2552	1089.8	156.8
6	5.46	4.66	.097	10.32	1162	2556	1109.9	159.7
7	5.40	4.72	.110	10.17	1170	2574	1134.2	163.2
8	5.36	4.78	.122	10.05	1170	2574	1148.1	165.2
9	5.30	4.87	.141	9.88	1170	2574	1168.3	168.1
10	5.22	4.97	.161	9.67	1160	2552	1182.9	170.2
11	5.14	5.06	.179	9.50	1156	2543	1199.6	172.6
12	5.06	5.14	.195	9.36	1142	2512	1203.0	173.1
13	5.04	5.18	.202	9.28	1140	2508	1211.4	174.3
14	5.02	5.20	.206	9.25	1124	2473	1198.2	172.4
10 ppm hydrogen; original measured, width-5.89 in., length-4.34 in. (Photo 1)								
4	5.88	4.40	.014	11.22	1228	2700	1081	155.5
5	5.84	4.52	.041	10.92	1228	2700	1109	159.5
6	5.78	4.63	.065	10.68	1240	2728	1147	165.0
7	5.73	4.72	.084	10.46	1248	2744	1179	169.7
8	5.65	4.82	.105	10.24	1256	2760	1210	174.1
9	5.57	4.94	.129	10.00	1258	2763	1242	178.7
10	5.42	5.11	.163	9.67	1256	2760	1282	184.5
11	5.31	5.23	.186	9.46	1256	2760	1309	188.4
150 ppm hydrogen; original measured, width-5.74 in., length-4.23 in. (Photo 17)								
20	5.68	4.30	.016	11.18	1260	2768	--	--
23	5.62	4.40	.039	10.93	1260	2768	--	--
26	5.55	4.50	.062	10.70	1268	2784	--	--
28	5.50	4.58	.079	10.49	1270	2793	--	--
30	5.43	4.65	.095	10.35	1274	2800	--	--
32	5.38	4.74	.114	10.12	1278	2808	--	--
33	5.34	4.77	.120	10.07	1282	2820	--	--
34	5.31	4.85	.137	9.91	1284	2823	--	--
35	4.30	4.89	.145	9.83	1284	2823	--	--

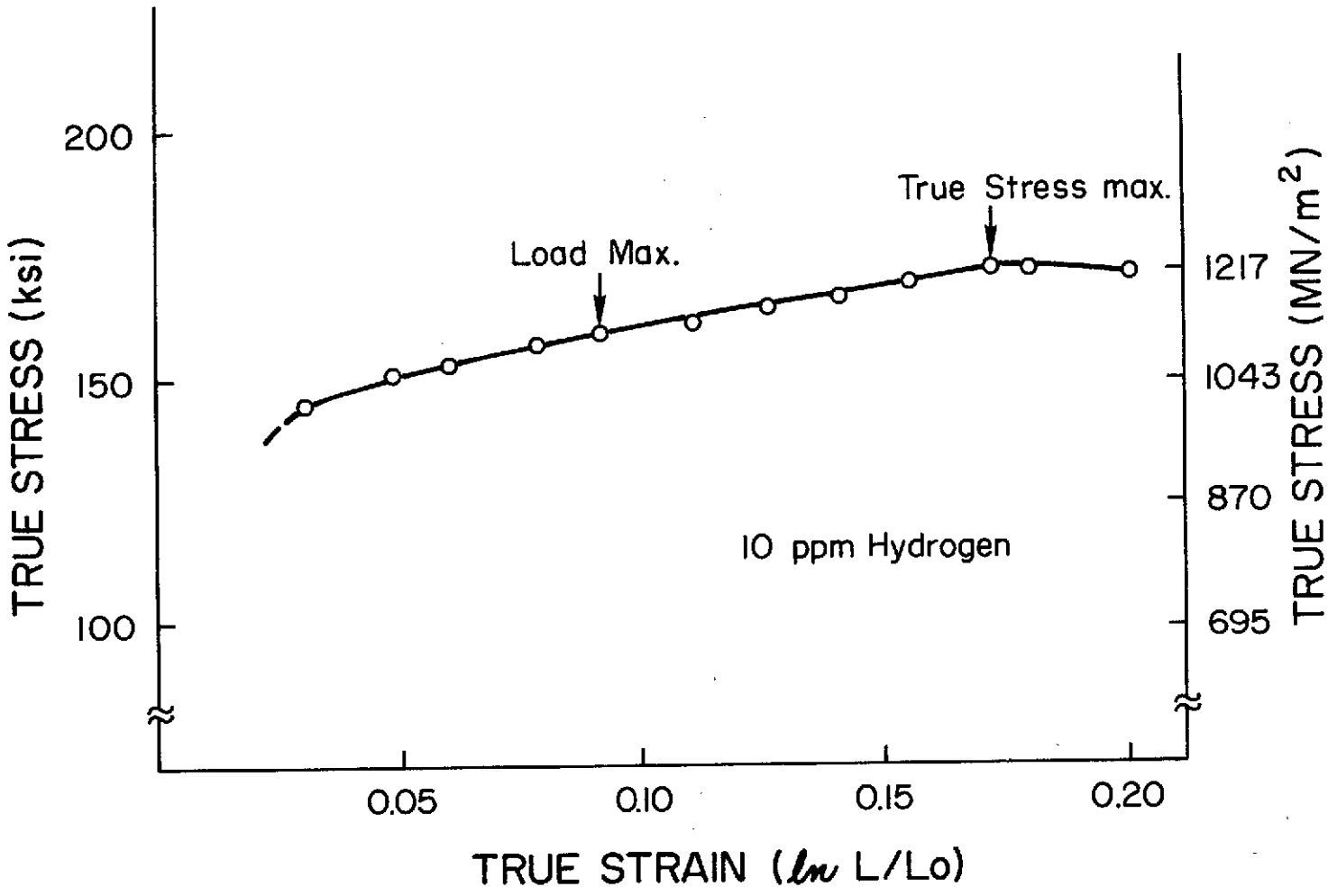

Fig. 12. True stress vs true strain for Ti-8Al-1Mo-1V with strain rate 0.14 min^{-1}

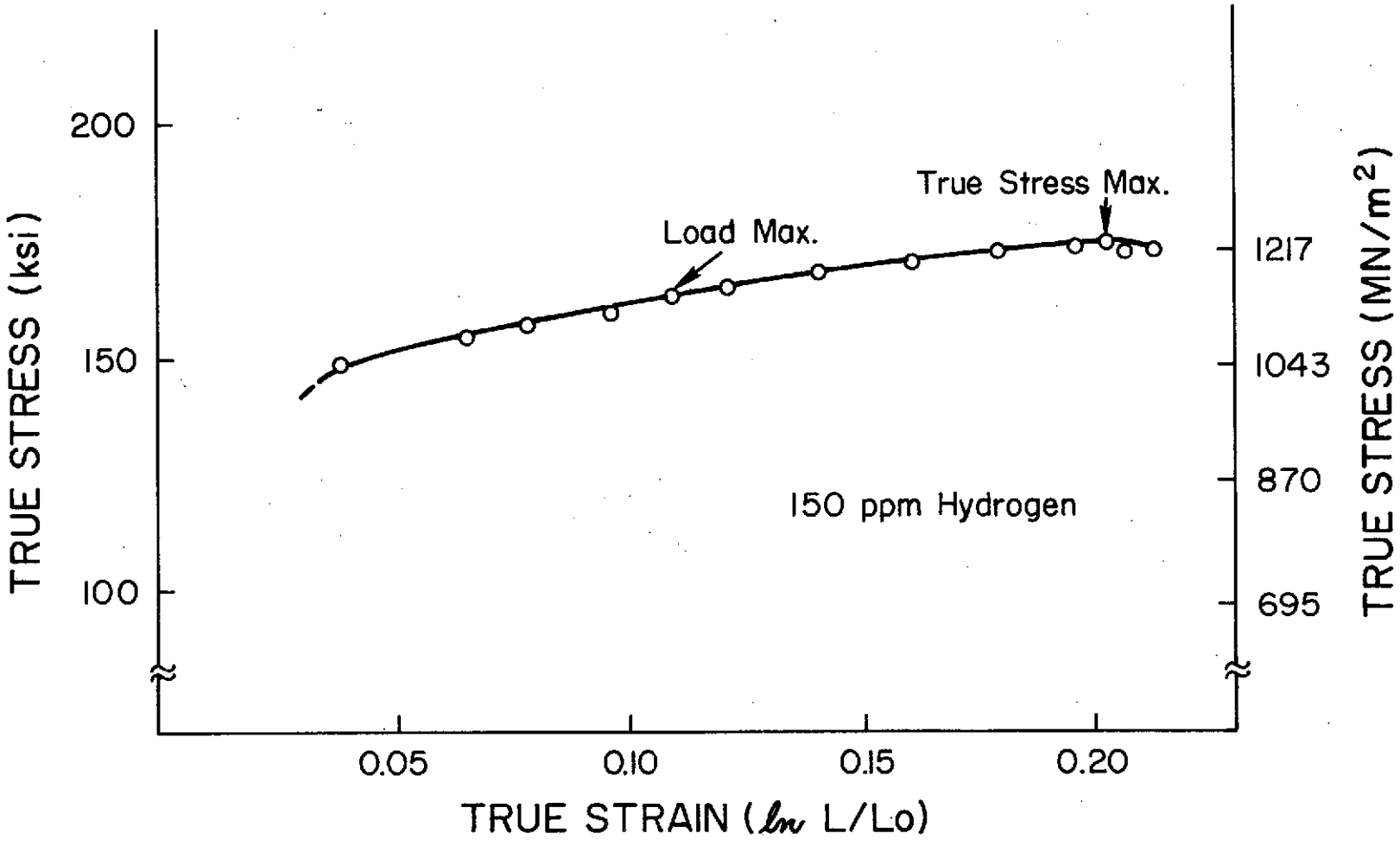

Fig. 13. True stress vs true strain for Ti-8Al-1Mo-1V with strain rate 0.14 min^{-1}

the tests once again show a true stress maximum. The important strain parameters from these tests were recorded and are shown in Table VI.

Table VI. Strain Parameters as Affected by Hydrogen Concentration Ti-8Al-1Mo-1V Alloy

Crosshead Speed 0.2 cm/min; Strain Rate 0.140 min^{-1}

	Hydrogen Concentration (ppm)		
	10	80	150
Strain at $d\sigma = 0$	.171	.189	.202
Strain at Disruption	.199	.216	.212
True Stress at Disruption (MN/m^2)	1194	1201	1199
(ksi)	172.0	173.0	172.4

The fracture pattern was quite different than in previous tests. The specimens showed definite mixed fracture modes, a combination of plane stress and plane strain. The plane strain mode is denoted by a horizontal crack as predicted when $\sigma_2 = \frac{1}{2}\sigma_1$, and it is evident that the higher hydrogen concentration resulted in a higher percentage of the plane strain mode. This can be seen in the fractures shown in Figs. 14 and 15. The angles of plane stress fracture were much easier to measure than in previous tests. The concentrated shear fractures or instability fractures were at angles less than 36° as was expected from the large width-to-thickness ratio. Thus, in the center $\sigma_2 = \frac{1}{2}\sigma_1$, and at the edges σ_2 became smaller because of less constraint.

Another group of specimens tested were those which had been aged to produce the α_2 compound Ti_3Al. This compound has been shown to affect the fracture toughness of the titanium alloys.[50] Investigators have shown[47] that the precipitation of this compound has a small effect on the tensile or yield strength of the material. The data gathered in the present experiments revealed a significant increase in tensile strength and a decrease in ductility. The tensile strength of an unhydrogenated aged specimen was 1090 MN/m^2 compared with the 1012 MN/m^2 for an unaged specimen.

There was little noticeable difference in the hardness of the specimens as recorded by Knopp hardness measurements. The hardness of the unaged material was 410 KHN and the aged material was 448 KHN.

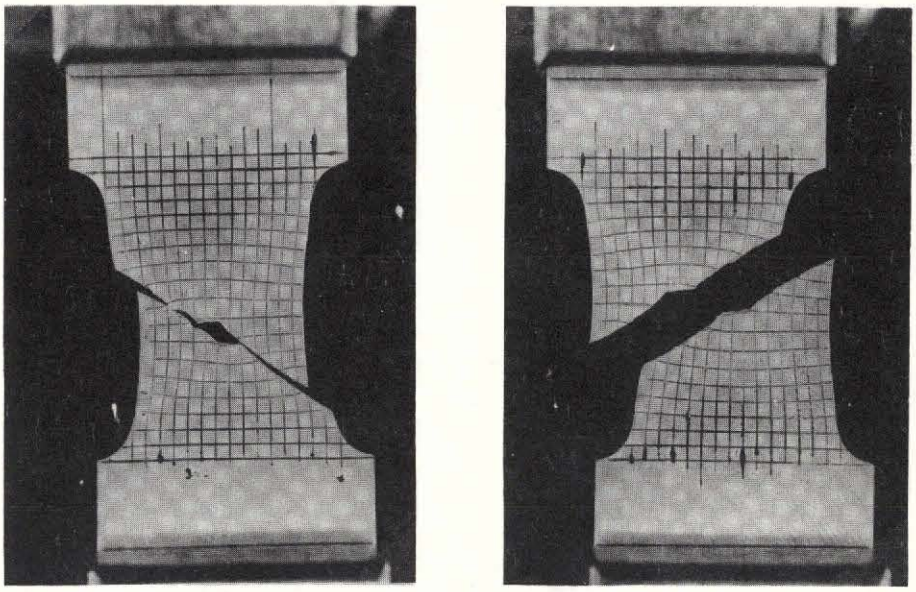

10 ppm hydrogen 80 ppm hydrogen

Fig. 14 - Fractures of Ti-8Al-1Mo-1V at 0.14 min^{-1} strain rate

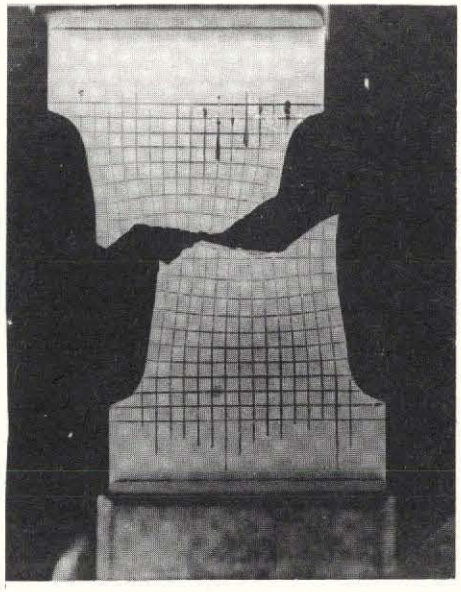

150 ppm hydrogen

Fig. 15 - Fractures of Ti-8Al-1Mo-1V at 0.14 min^{-1} strain rate

Table VII gives the strain parameters for the aged specimens, as determined from the measured values recorded in Table V. No true stress maximum was observed and all the specimens, regardless of hydrogen content, showed mostly a plane strain mode of fracture. Figure 16 shows two of the specimens broken. The specimen containing 80 ppm H_2 broke prematurely at a very low strain value. This fracture was directly related to a score mark on the surface and although the results are included in the table below, they will be excluded from further discussion.

To determine if texturing might play a part in the fracture phenomenon, samples were made having the tensile axis both 45° to the rolling direction and transverse to the rolling direction. The samples contained 10 and 150 ppm of hydrogen. The strain parameters found are shown in Table VIII (the capsule containing the transverse bar at 10 ppm broke in the furnace so no data were obtained for the 10 ppm specimen).

Table VII. Strain Parameters for Ti-8Al-1Mo-1V Aged to Produce Ti_3Al Compound

Strain Rate 0.14 min^{-1}

	Hydrogen Concentration (ppm)		
	10	80	150
Strain at Disruption	.186	.065	.145
True Stress at Disruption (MN/m^2)	1310	1123	1292
(ksi)	188.4	161.5	185.7

Table VIII. Strain Parameters for Ti-8Al-1Mo-1V as Affected by the Rolling Direction

	10 ppm Hydrogen			150 ppm Hydrogen		
	Trans.	45°	Long.	Trans.	45°	Long.
Strain at $d\sigma = 0$	-	.203	.192	.167	.202	.222
Strain at Disruption	-	.213	.216	.209	.246	.246
Stress at Disruption (ksi)	-	156.9	169.8	173.1	167.6	181.7
(MN/m^2)	-	1089	1180	1205	1164	1263

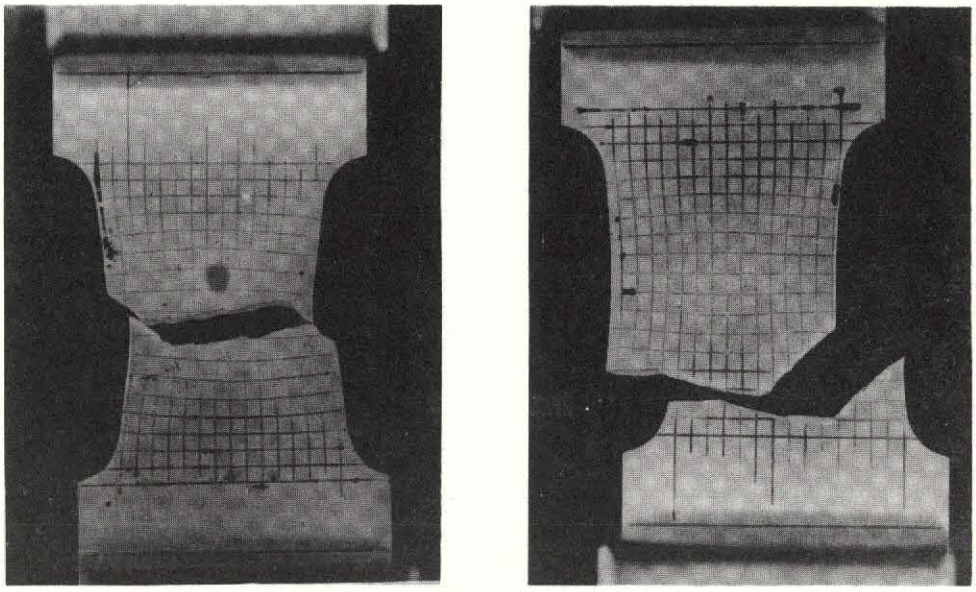

10 ppm hydrogen

150 ppm hydrogen

Fig. 16. Fracture of aged Ti-8Al-1Mo-1V with strain rate of 0.14 min^{-1}

DISCUSSION

Ti-5Al-2.5Sn ALLOY

As can be seen from Figs. 7 and 8, the flow stress increased with the addition of hydrogen. This would be in agreement with data reported by many observers. The strain at the maximum true stress or at the onset of instabilities increased with increasing hydrogen except for the highest hydrogen level. This would seem to indicate that the hydrogen was hindering the onset of instabilities. This is opposite to what might have been predicted if hydrogen had acted as a "plasticizer" in titanium. If this had been the case, hydrogen would have caused instability onset at lesser strain values. This could be predicted from the fact that the instability failures depend on the plastic character of the material.

If the material were made more plastic, it might be expected to strain harden to the point of exhaustion sooner and at this point become ideally plastic and fail along characteristics in an unstable manner. It has been shown that in low interstitial titanium one slip plane is active (1011); but in higher interstitial titanium (O_2 and N_2 being the interstitial elements) all three slip planes are nearly equally favored.[51] It was thought that the effect of hydrogen at interstitial sites in the titanium lattice was to expand the lattice in directions such that more slip planes could be activated. This does not appear to be the case and no known literature is available to show how interstitial hydrogen affects the resolved shear stress.

A log-log plot of the flow stress data for the 0.1575 min^{-1} strain rate specimens is shown in Fig. 17. The curves reveal no real trend as to the effect of hydrogen on the strain hardening exponent.

One thing that is evident is that the greater the hydrogen concentration, the less tolerance the material has for the instability (Fig. 18). Thus, the higher the hydrogen the sooner failure occurs after the instability onset or the smaller is the value for strain at $d\sigma = 0$ minus strain at disruption.

A typical fracture sequence for center crack initiation is diagrammed in Fig. 19. "A" shows the initial stages of straining and "B" represents the deformation bands which initiate at certain points in the plastic deformation region of the stress-strain curve. These bands were originally at an angle of approximately 36° with the horizontal. From theories of Kobayashi[52] this would indicate that the stress state in the specimen was uniaxial. This means that there is no σ_2 initially. Kobayashi developed formulas for determining slip line directions for the plane stress condition. When a uniform state of stress is assumed these formulas become

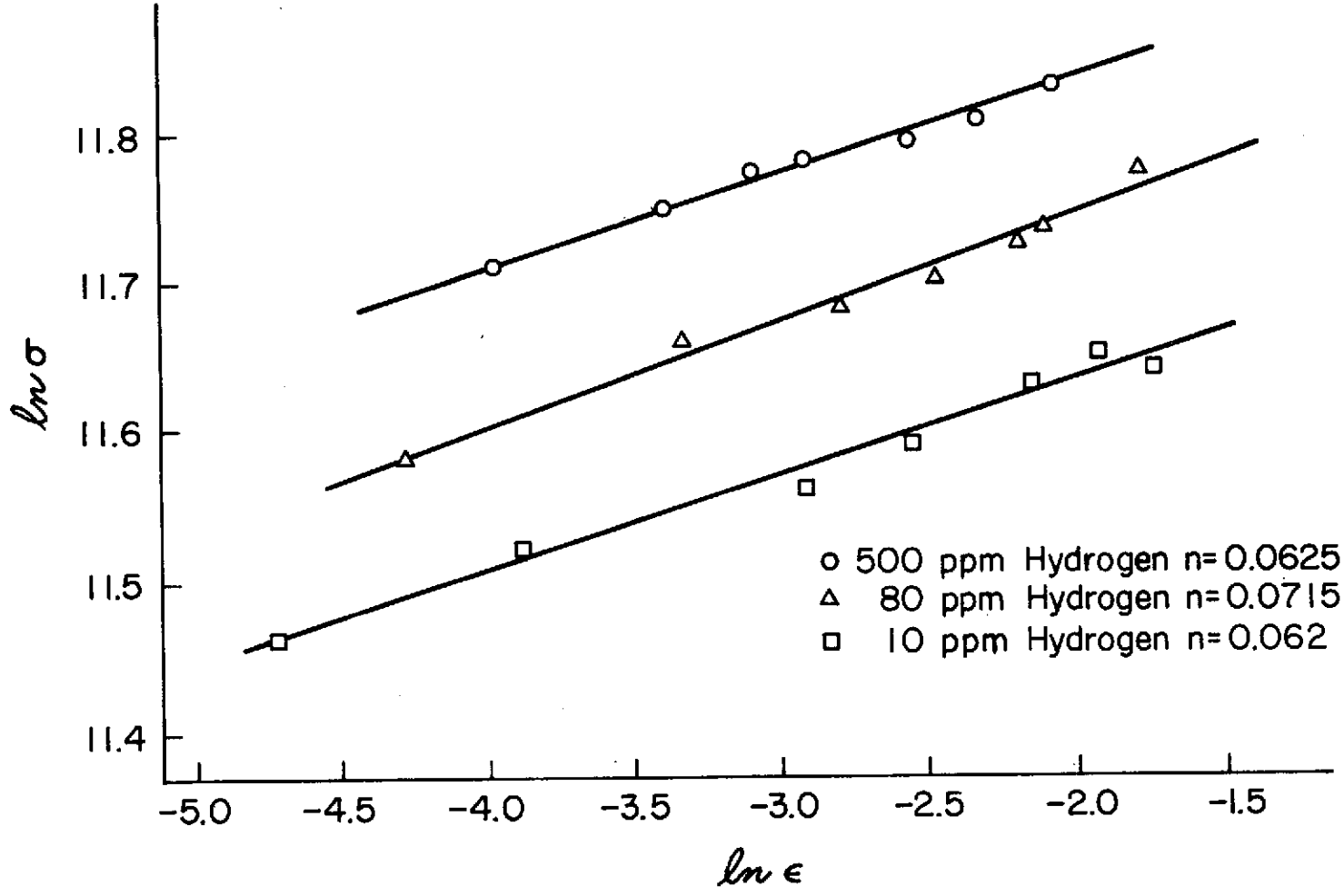

Fig. 17. Log true stress vs log true strain for Ti-5Al-2.5Sn

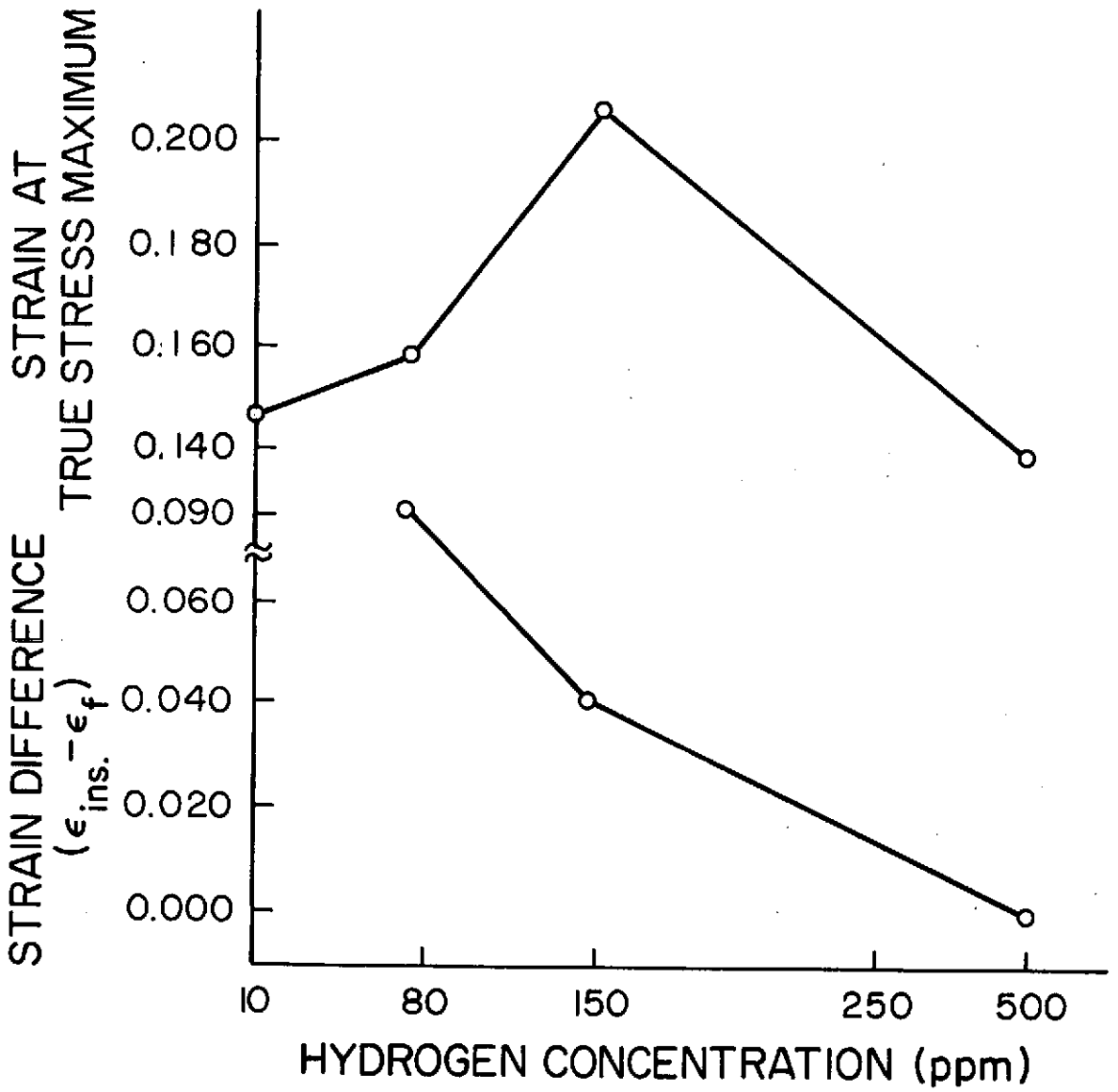

Fig. 18. Strain parameters for Ti-5Al-2.5Sn with strain rate 0.1575 min^{-1}

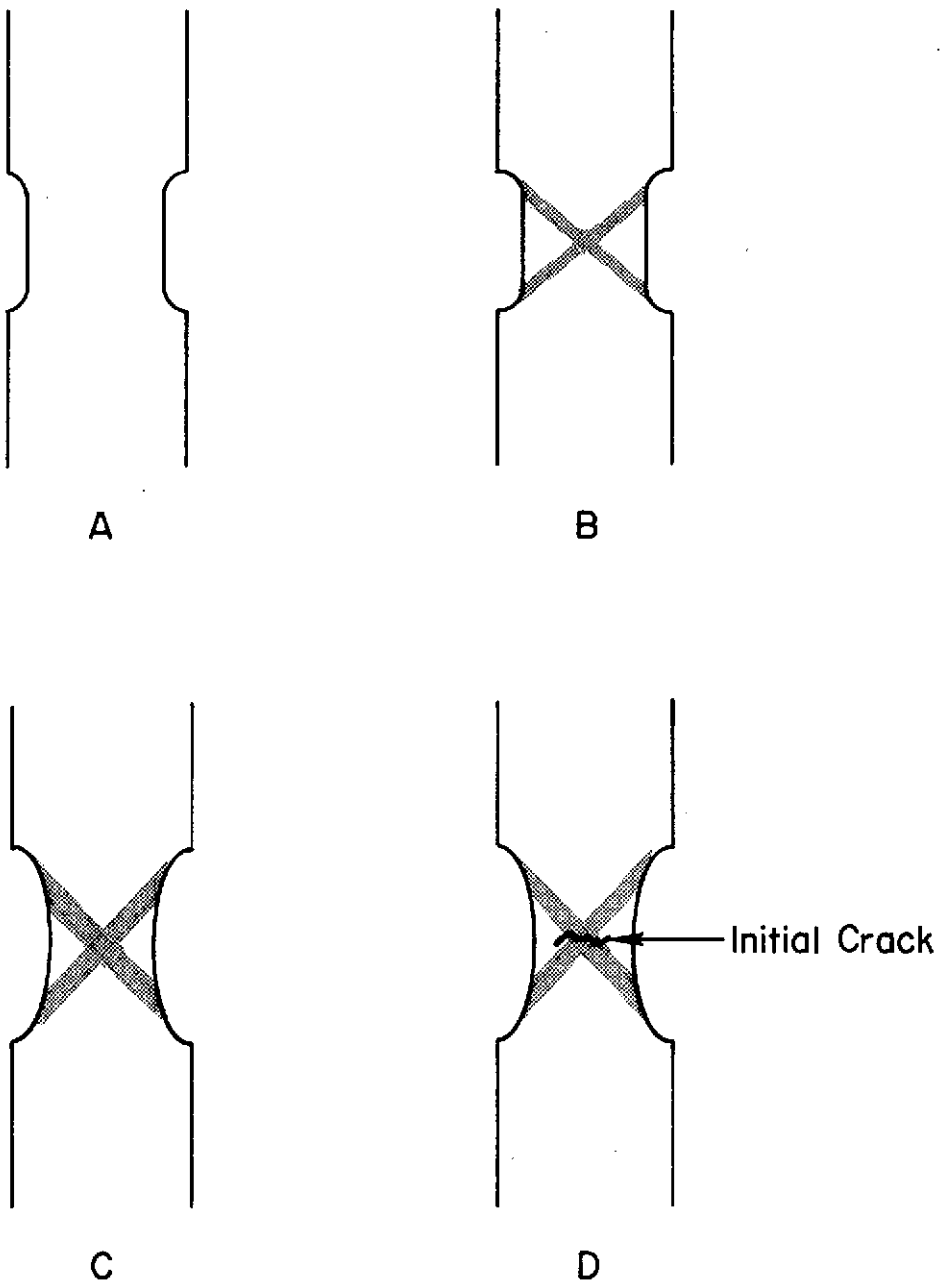

Fig. 19. Typical fracture pattern for separation at the center of a tensile specimen

$$\theta = \pm\left(\frac{\pi}{4} + \frac{\psi}{2}\right),$$

where θ is the angle between the slip lines and the principal stress direction (σ_1), and

$$\sin \psi = \frac{1}{3} \frac{\sigma_1 + \sigma_2}{\sigma_1 - \sigma_2}.$$

This predicts that when $\sigma_2 = 0$, $\theta = 54° 44'$ and when $\sigma_2/\sigma_1 = \frac{1}{2}$, $\theta = 90°$. The formation of the bands in the present study was associated with either the start of plastic deformation or the maximum load point, and definitely not associated with the true stress maximum. The instability formation, which may have occurred at the true stress maximum, was within these deformation bands.

Stage "C" shows the deformation band widening and at stage "D" a running crack occurred which covered about one-half the specimen width. After this crack was arrested the continuance of loading caused a slow tearing until final edge shear resulted in complete separation. An example of the load vs extension plot corresponding to this failure is shown in Fig. 20. The disruption stage can be seen in each of the load curves at the first crack appearance.

Parker[53] has shown a detailed diagram of fracture (in a ductile material) which was identical to the behavior in this experiment. He explained that the stepped pattern in the high shear stress regions at the central part of the specimen consisted of steps making angles of 45° or less with the specimen axis. While it is not easy to accurately measure these short steps, they appear never to be more than 40° in this experiment. Therefore, these angles do not necessarily support the argument that the fractures occur on planes of maximum shear stress.

When the failed specimen sections were mounted and polished it became immediately obvious that pore formation was occurring. The greatest concentration of pores was found in the central part of the specimen where triaxial stresses were greatest. This triaxial state of stress enhances pore formation. Pore formation and coalescence is a common failure mode and it had been the intention of these experimental methods to inhibit this type of failure mode.

It is believed that pores which formed and grew in this material became the initiation sites for the plastic instability mode of failure. Thus, failure was due to the third type of instability flow as described in the literature review. Load disruption did occur in each test with the formation of an unstable crack. This crack was not at angles of maximum shear stress but more nearly along angles determined by plasticity theory. The pores provided the stress gradient and free surface

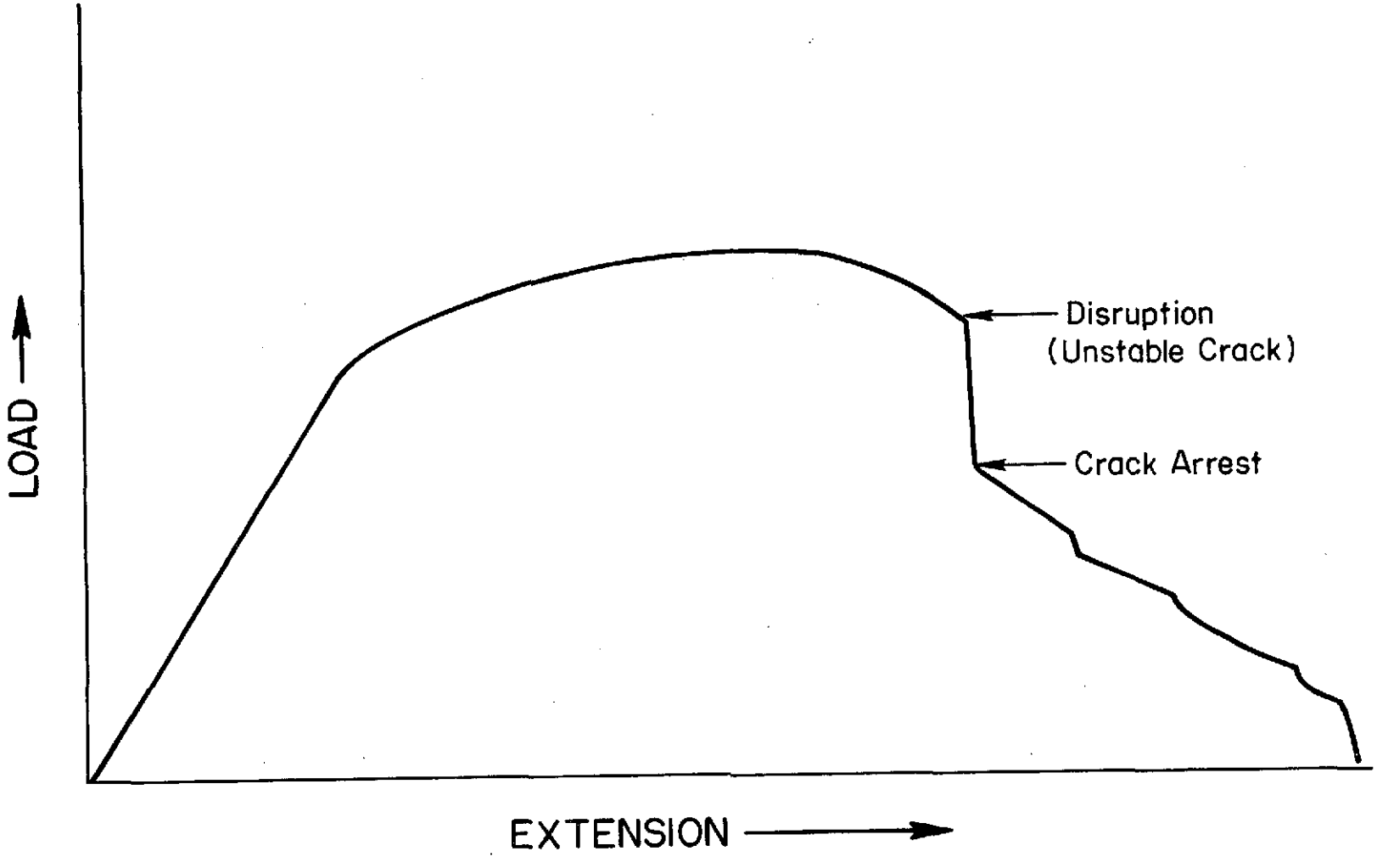

Fig. 20. Typical load-extension curve for Fig. 21 fracture

necessary for instability formation. The crack propagated through the area of highest shear stress (smallest cross-section due to necking) but was arrested in the area of lower shear stress. From that point the specimens failed because of a slow tear (pore formation and coalescence) until final shear at the edges occurred.

Metallographic examination of the pores showed that they were associated with grain boundaries and may well have been enhanced by possible hydrogen partitioning in the boundaries. They were definitely associated with grain boundary particles and, although it was not proven that these were oxides, it is suspected that they are oxides since this material as in any commercially available titanium contained about 0.1% oxygen content by weight. Figure 21 shows the particles and the voids they caused.

Ti-8Al-1Mo-1V ALLOY

In the Ti-8Al-1Mo-1V alloy it is evident, as with the first alloy discussed, that the strain at the true stress maximum increases as hydrogen concentration increases. Likewise, the tolerance for the instabilities decreases with increased hydrogen concentration, as shown in Fig. 22. Thus, once the instability forms in the 150 ppm hydrogen specimen, failure occurs sooner than in the 10 ppm specimen. Not as evident as before are changes in the flow stress, which appears to change very little with increasing hydrogen.

To determine how accurate the strain data were using ℓn L/Lo, the final strain was compared to that calculated strain using the final measured width and thickness (ℓn Ao/A). The results were very good, as shown in Table IX.

The tensile sheet specimens were originally designed in an attempt to produce both a plane stress and a plane strain state of stress. Torsional specimens, which have been used successfully for several years to show instability formation, have at their surface this same state of stress (plane strain and plane stress). In the tensile specimens the plane strain state exists when $\sigma_2 = \frac{1}{2}\sigma_1$. This can be shown by looking at the equation for width strain in the plastic deformation region of the flow curve. The equation is

$$\epsilon_2 = \frac{1}{P}\left(\sigma_2 - \nu\sigma_1\right),$$

where P is the plastic modulus and, in plasticity, ν (Poisson's ratio) is $\frac{1}{2}$. Thus, $\epsilon_2 = 0$ when $\sigma_2 = \frac{1}{2}\sigma_1$. The plane strain state results in the coincidence of directions of pure shear and maximum shear stress, both in the direction of σ_2. Thus, a horizontal fracture results.

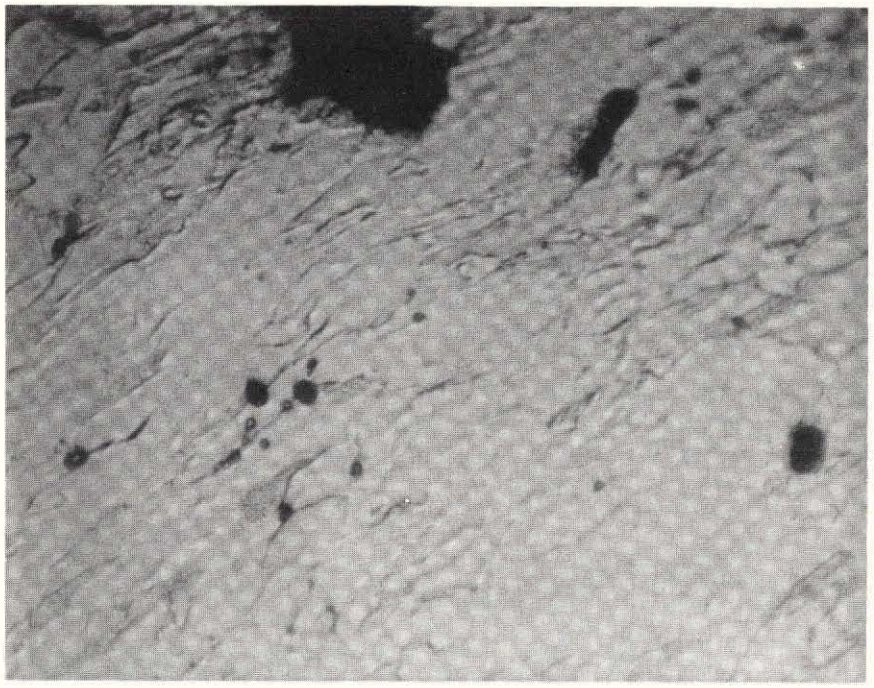

NOTE: Possible oxide particles can be seen in lower left quadrant. The large black area at top is the edge of the fracture.

Figure 21 - Void formation in a Ti-5Al-2.5Sn specimen related to particles in the grain boundaries 500X

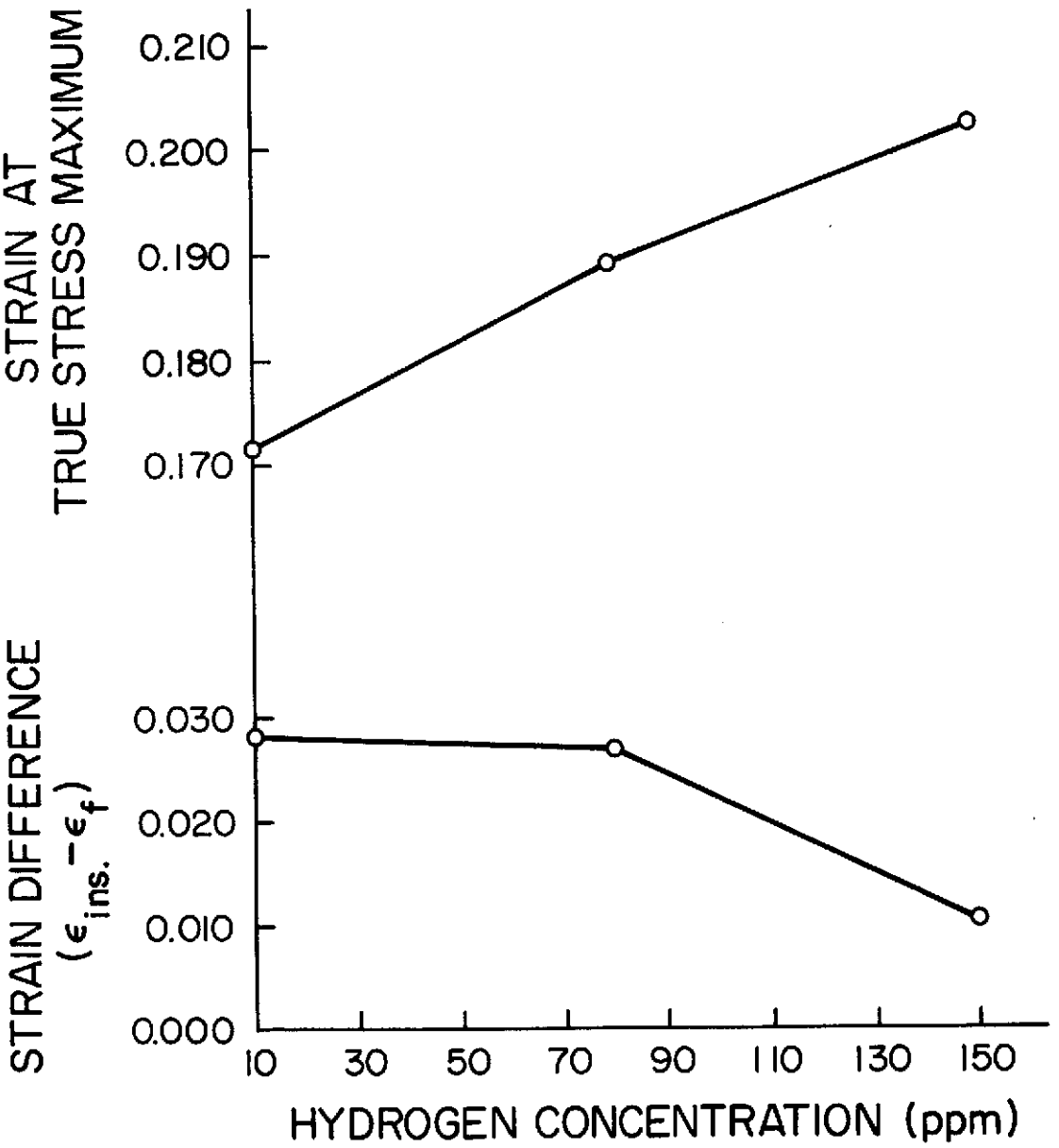

Fig. 22. Strain parameters for Ti-8Al-1Mo-1V

Table IX. Comparison of Final Strain Using $\ell n L/Lo$ and $\ell n Ao/A$

Specimen	Original Area (mm^2)	Final Area (mm^2)	Final Strain ($\ell n Ao/A$)	Final Strain ($\ell n L/Lo$)
Ti-8-1-1 10 ppm hydrogen	11.41	9.32	.202	.199
Ti-8-1-1 80 ppm hydrogen	11.41	9.15	.221	.216

It is apparent from Figs. 14 and 15 that as the hydrogen concentration increased the specimens showed greater degrees of plane strain fracture. These horizontal fractures were slanted from front to back whereas the remaining inclined fractures were not. Slant fractures in failure analysis are often incorrectly determined to be ductile fracture shear lips. This familiar slant fracture was determined in this study to be the plane strain mode.

Table X shows the angle between the inclined fracture and the horizontal axis, and it can be seen that, in general, the existence of hydrogen caused a decrease in the angle. It is not understood why the angle did not continue to decrease gradually between 80 and 150 ppm hydrogen. Others[37] have shown a minimum angle of about 28° before complete horizontal fracture occurred, and it appeared as the same type of a phenomenon as is related to this alloy. It seems that a gradual decrease in the angle or a sudden decrease (as in this case) depends on which flow condition (Tresca or Von Mises) the material follows.

Table X. Angles of Instability Formation

Hydrogen Concentration (ppm)	Angle Between Fracture Plane & Horizontal Axis (°)
10	33-34
80	32
150	32

No real explanation can be made as yet to explain the increased total strain resulting from hydrogen concentration increases. Boyd et al.,[47] using tensile sheet specimens, showed that the presence of even enough hydrogen to produce strain-induced hydrides (> 200 ppm) does not affect the ductility of Ti-8Al-1Mo-1V. Actually the ductility increased with higher hydrogen concentration regardless of the strain rate

used (they used 3/min and 3 x 10^{-3}/min strain rates). Only when spontaneous hydrides were precipitated did ductility decrease. These data agree fairly well with those generated in this report. Total strain and reduction in area data for the Ti-8Al-1Mo-1V used in the present experiment are shown in Table XI.

Table XI. Ti-8Al-1Mo-1V Ductility Data

Hydrogen Content (ppm)	10	80	150
Total Strain at Disruption	.199	.216	.212
Reduction in Area (%)	17.3	20.0	19.0

Schwartsberg[54] has shown drastic effects of slow strain rates on reduction of area properties in some titanium alloys (Ti-140A). His data indicated a drop in reduction area from 60 to 12% for testing speed change from 1.0"/min to .005"/min in an alloy (α-β) containing 500 ppm hydrogen. Yet Lenning's data[46] for α-titanium alloy showed an increase in reduction area. Thus, the amount of β phase seems to be significant.

An attempt was made to obtain samples for transmission microscopy but for the most part the attempt was futile. A very small area of one 150 ppm hydrogen sample was examinable and no strain-induced hydrides were found: but in general it is not possible to say whether or not strain-induced hydrides existed in the lower hydrogen concentrations.

From examination of the flow curves in Figs. 12 and 13 it is seen that hydrogen has no noticeable effect on the strain hardening coefficient of Ti-8Al-1Mo-1V alloy. Boyd et al.[47] had shown a strain-hardening effect, but his hydrogen concentrations were considerably higher than those used in this study.

Comparison of the aged and unaged Ti-8Al-1Mo-1V alloy revealed that the aging treatment resulted in a significant increase in strength and a decrease in ductility. Figure 23 shows the strain-hardening exponents for the 10 ppm hydrogen samples. The aged specimen has a lower strain-hardening exponent than does the unaged specimen. Chakrabarti[37] has shown that instability formation is easier the lower the strain-hardening exponent. Chakrabarti's work was on 4340 steel and may not be applicable to other material systems. Since no true stress maximum was obtained for the aged specimens in the present study, it is not possible to determine the effect of the strain-hardening exponent on instability formation. The only speculation that can be

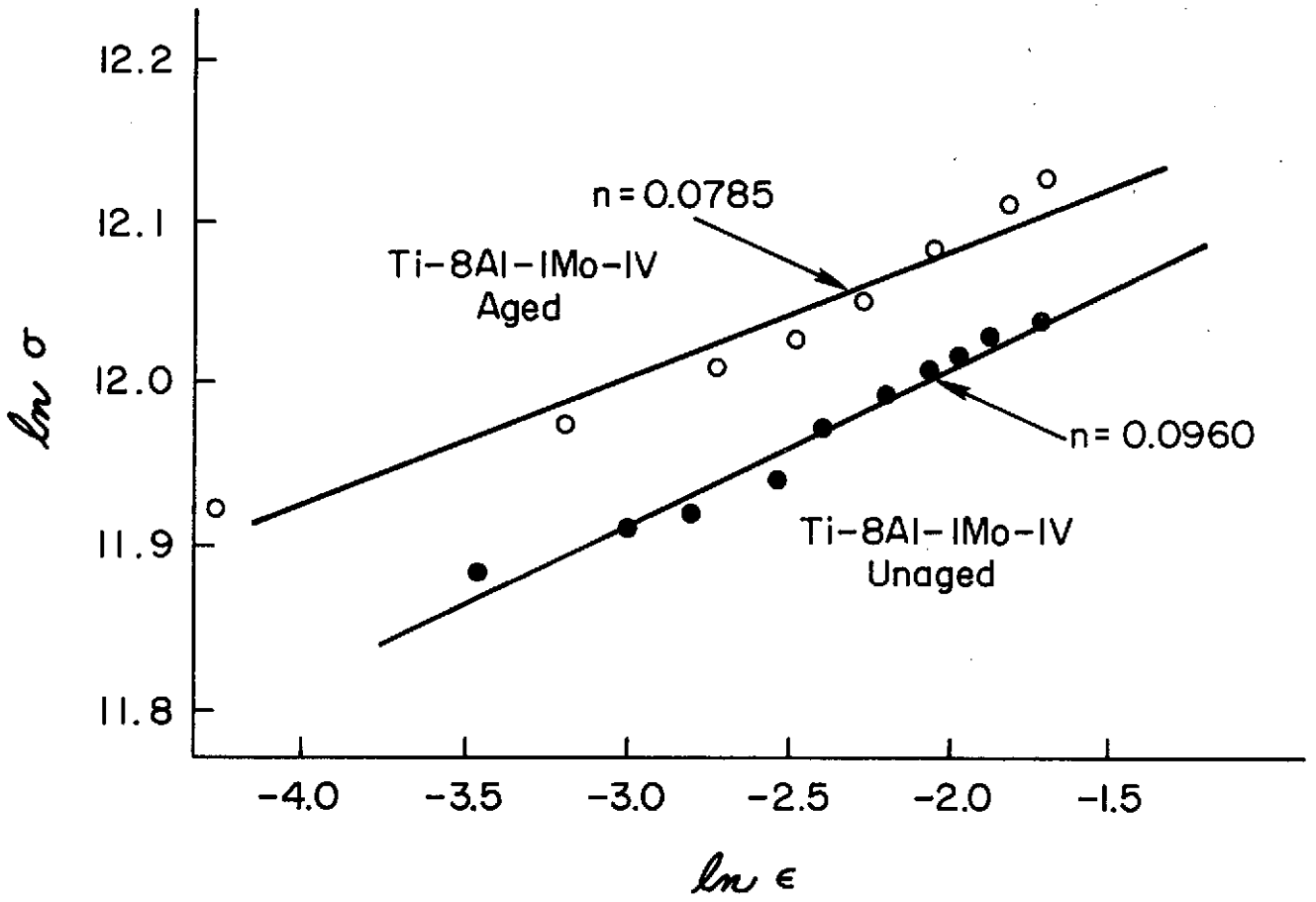

Fig. 23. Log true stress vs log true strain

made is that if the aged specimens failed because of instability formation, they did so at a lower strain than the unaged specimens and they possessed no tolerance for the instabilities.

Examination of scanning electron microscope (SEM) fractographs in Figs. 24 and 25 show that much of the fracture was related to pore formation. Optical metallography showed very few pores near the fracture. One can notice in Fig. 24 that there are many flat areas connecting the pores. It is felt that the fracture of this material must follow the second type of instability controlled failure. This takes place when the plane of instability flow is thicker than the second-phase particles (in this case, β phase) and causes pore nucleation. This was quite evident in the microsample observed from the Ti-8Al-1Mo-1V specimen having 150 ppm hydrogen. The photomicrograph for this structure was not clear but a schematic is shown in Fig. 26. A very sharply defined deformation band was found at the small tip on either side of which there was very little or no deformation. In this deformed band were very small pores (much larger in the schematic than in reality) which had been elongated. These pores are believed to have been created by the instability flow.

The fractograph in Fig. 25 shows a finer structure than in Fig. 24, but both specimens showed a consistent structure over their entire surface whether on the horizontal or inclined part of the fracture. It is therefore apparent that the first crack initiated was unstable across the entire width. This can also be evidenced from the load-extension diagram which showed only one load disruption which lowered the load instantaneously to zero with no arrests.

The results of testing specimens taken in directions other than the rolling direction showed that the same phenomena occurred. Table VIII indicates that the higher hydrogen concentration produced higher disruption strains. There was some indication that less strain occurred when the specimen axis was transverse to the rolling direction. Fractures were similar to those found in the first tests and angles of separation were about 33°.

The effect of hydrogen on the strain rate sensitivity was investigated. Specimens having 10 and 150 ppm hydrogen were tested, with each test starting at a strain rate of 0.14 min^{-1}, and at approximately 0.03 strain the strain rate was changed to 1.4 min^{-1}. The load increased from 1176 to 1204 kg for the 10 ppm hydrogen specimen, and from 1256 to 1300 kg for the 150 ppm specimen. The strains used were much lower than the strain for necking so that necking caused no inaccuracies. The strain rate sensitivity "m" could be calculated from the relationship

$$m = \frac{\ell n \sigma_2/\sigma_1}{\ell n \epsilon_2/\epsilon_1} .$$

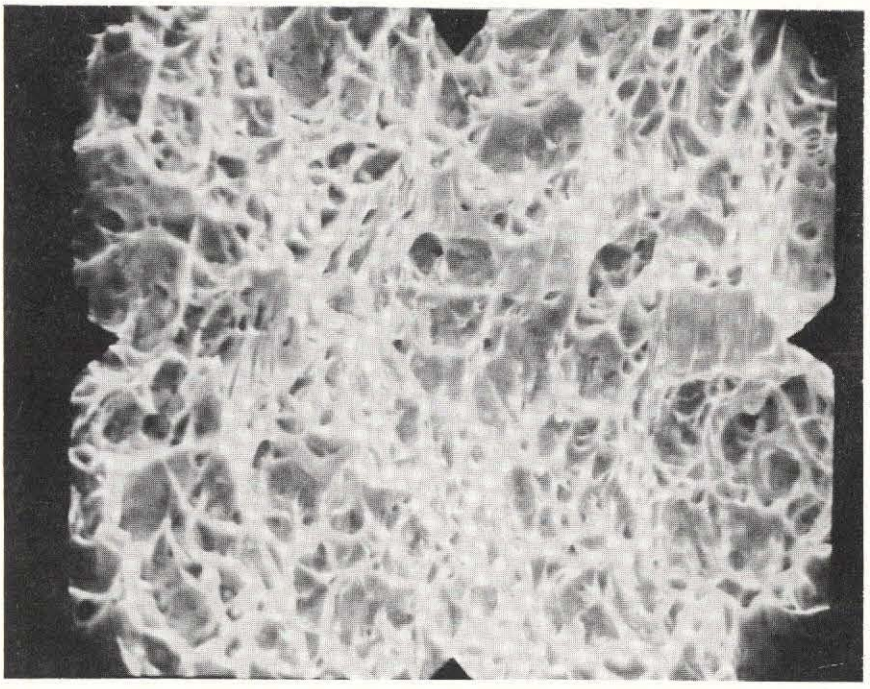

Fig. 24 - Fracture surface of unaged Ti-8Al-1Mo-1V specimen containing 10 ppm hydrogen
SEM 1000X

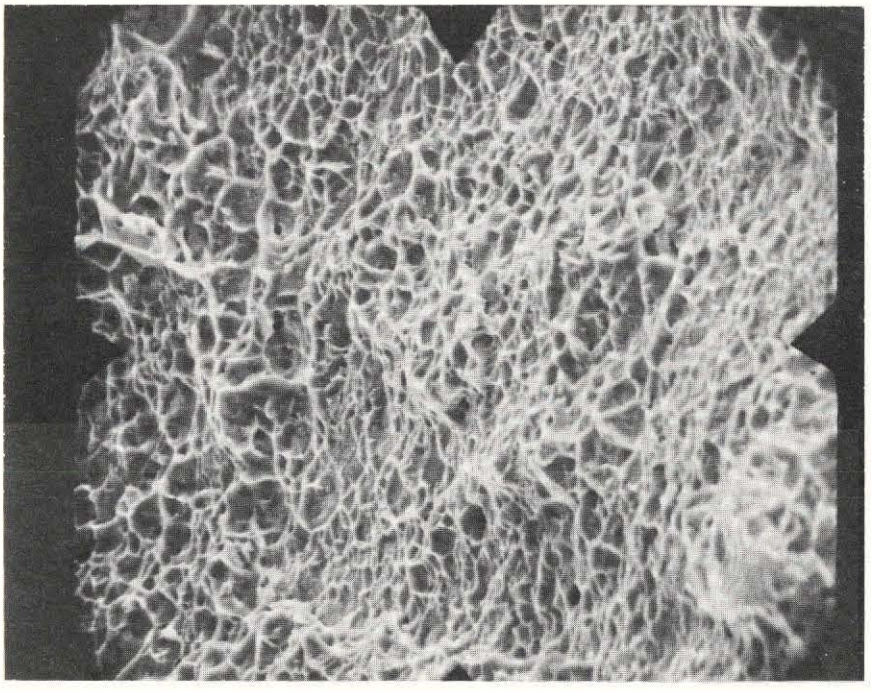

Fig. 25 - Fracture surface of aged Ti-8Al-1Mo-1V specimen containing 10 ppm hydrogen
SEM 1000X

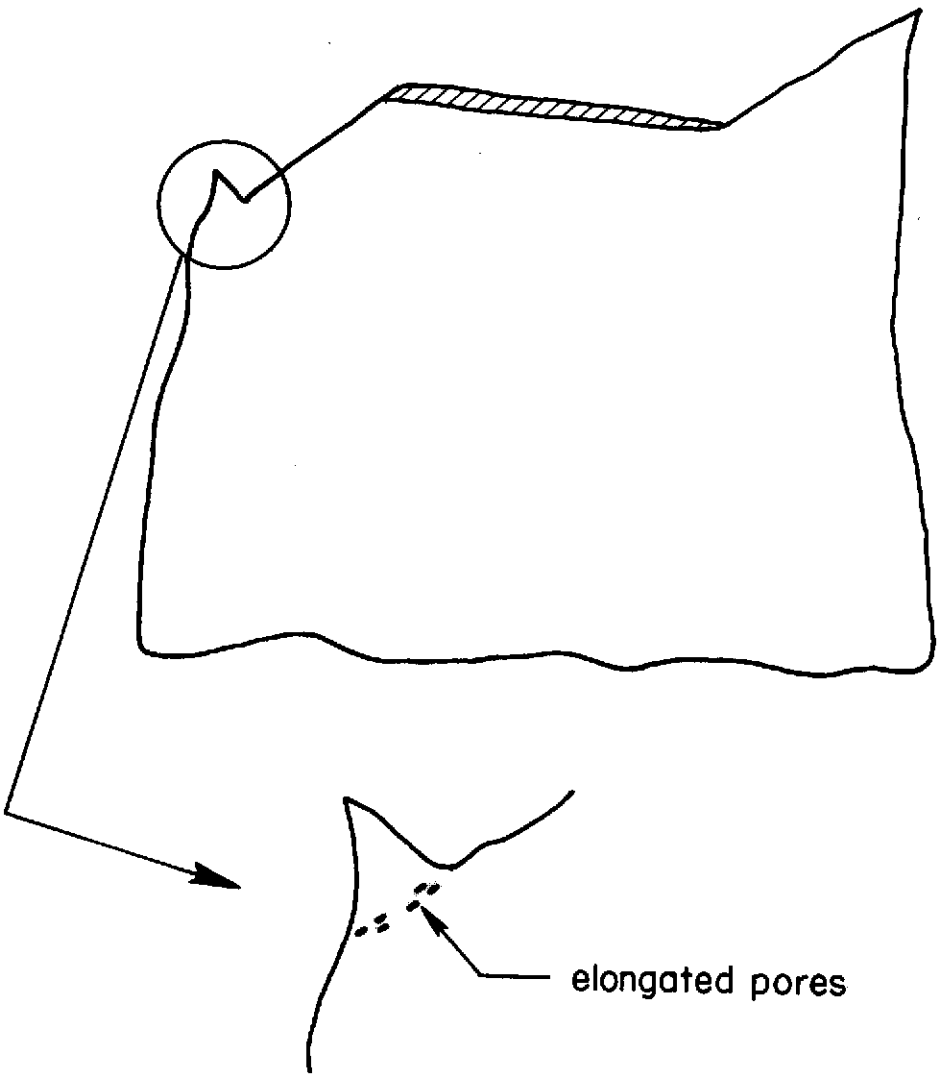

Fig. 26. Schematic of Fig. 17A showing thick instability flow band and the pores nucleated in it

The results gave a value of m = .0099 for 10 ppm hydrogen and m = 0.0145 for 150 ppm hydrogen. Thus, increasing the hydrogen concentration from 10 to 150 ppm resulted in a 46% increase in the strain rate sensitivity exponent.

This observation furnishes a rationale for stabilization of the α-Ti alloys against the shearing instability. According to the necessary condition for onset of this type of instability

$$d\sigma = \left(\frac{\partial\sigma}{\partial\epsilon}\right)d\epsilon + \left(\frac{\partial\sigma}{\partial\dot{\epsilon}}\right)d\dot{\epsilon} + \left(\frac{\partial\sigma}{\partial T}\right)dT = 0 .$$

Increasing strain hardening and increasing strain rate sensitivity will increase the strain at instability, whereas increasing the adiabatic heating contribution to the flow stress will decrease this strain. The tensile data indicate no significant effect of hydrogen on strain hardening capacity. The constant specimen geometry and rate of straining furnishes no expectancy of a change in the adiabatic heating. Therefore, it must be concluded that hydrogen increases the strain to instability through the effect on strain rate sensitivity.

It is not known exactly how interstitial hydrogen affects the slip system in titanium. If it behaves as other interstitials (oxygen or nitrogen) it might be expected to increase the number of slip planes. Thus, dislocation ovement might be made easier, leading to easier dislocation interaction, the result being increased strain hardening. As the dislocation density increases the periodicity of the atoms decreases.[42] Therefore, when the strain hardening is exhausted the atoms can flow over each other in directions dictated by continuum plasticity theories, and are not necessarily confined to movement in crystallographic directions. In this high degree of disorder hydrogen might be expected to aid flow and to cause it to occur sooner. Thus, the localization of flow would occur at a lower strain rate with hydrogen present.

On the other hand if hydrogen hindered the dislocation movement, it would cause the titanium to have less strain-hardening capacity, resulting in faster exhaustion of strain hardening and a lower strain for plastic instability formation.

From this study, it appears that hydrogen does affect the plasticity of the titanium alloys used. The result being to increase the total strain as hydrogen concentration is increased. When the hydrogen concentration reaches that necessary for spontaneous hydride precipitation the total strain decreases. The material is first affected while it is deforming as a crystallographic solid. Hydrogen seems to prolong uniform deformation and prevent the unstable straining associated with very localized cross section fluctuations. Thus, in Figs. 12 and 13 the maximum load point (usually associated with the diffuse necking phenomena) occurs at a higher strain with increased hydrogen.

Hydrogen forestalls localization of plastic flow into narrow deformation bands, but allows or forces it to occur over a wider area. The resulting instability flow initiates at higher rather than lower strains. Once localization and instability flow do occur, hydrogen aids the instability flow causing instability fracture to occur sooner with increased hydrogen concentration. This suggests that anything which helps to localize plastic flow in the presence of a high hydrogen concentration will aid in instability formation. Therefore, notches and hydride precipitates would tend to localize the plasticity and cause instability flow. The introduction of the α_2 compound could lower the diffuse ductility to the point where localization occurs faster and there is no tolerance for the instability.

The occurrence of ever-increasing amounts of plane strain mode with increasing hydrogen content, as shown in Figs. 14 and 15, may be explained by the interaction of the deformation regions. If hydrogen increased overall slip, as observed, then it might be expected that σ_2 would rise over a wider distance as σ_1 increased. It turned out that the interaction of the deformation bands was directly related to the amount of plane strain mode present, as shown schematically in Fig. 27. "A" shows a narrow interaction region and a small plane strain fracture; "B" and "C" show increasing interaction regions and larger plane strain fractures.

Relative to the stress corrosion of titanium the phenomenon of instability flow could predict that there is a critical strain at the notch at which unstable flow occurs. The hydrogen absorbed into the lattice at this notch root would increase the plasticity of the material and cause instability flow to occur sooner than if the environment produced no hydrogen.

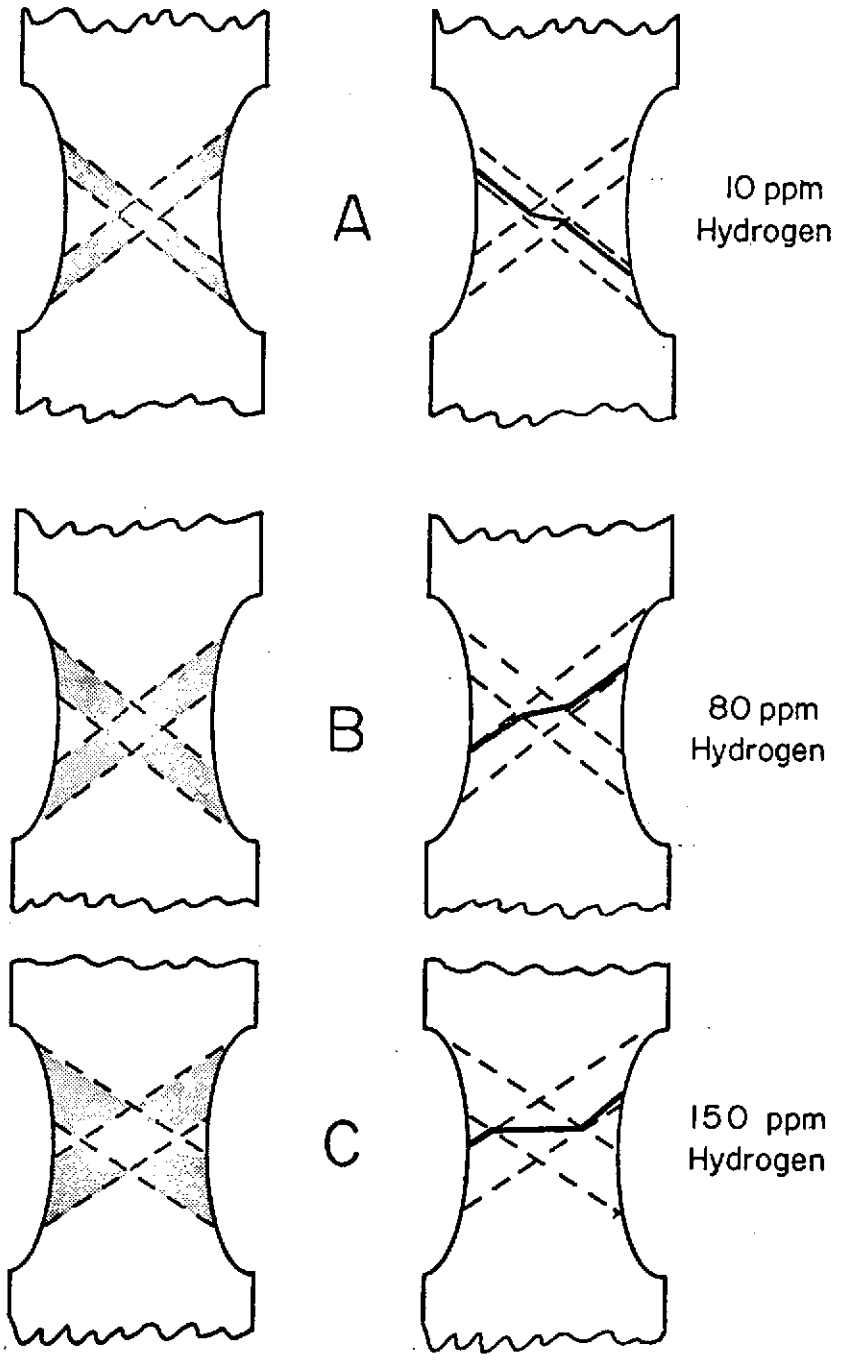

Fig. 27. Schematic of the interaction of major deformation bands and the fracture pattern produced

CONCLUSIONS

1. In most cases the effect of hydrogen, in concentrations less than those necessary for spontaneous hydride precipitation, was to increase the strain necessary for any given event (instability formation or instability failure). The increase in strain instability is attributed to the increase of strain rate sensitivity with increasing hydrogen content.

2. The titanium alloys used showed a decreasing tolerance for instability, once it forms, with increasing hydrogen concentration, or in other terms, hydrogen increases the strength of the instability.

3. The strain-hardening exponent for the titanium alloys used, particularly the Ti-8Al-1Mo-1V, was not significantly affected by different hydrogen concentrations. The strain rate sensitivity seemed to be increased by increased hydrogen concentration.

4. The presence of the spontaneous hydrides or the Ti_3Al compound lowered the total strain to fracture and the strain necessary for instability formation.

5. Results of the tests performed on the Ti-8Al-1Mo-1V alloy indicated that an instability flow mechanism was controlling the fracture. The second type of instability control is thought to be operative.

6. Hydrogen increased the amount of plane strain mode fracture in the Ti-8Al-1Mo-1V material.

7. Failure of the Ti-5Al-2.5Sn alloy appeared to be caused by instability flow connecting large pores in the specimen.

8. The Ti-5Al-2.5Sn (ELI) alloy, regardless of its single-phase matrix, is not a good material to work with using the sheet tensile specimen. The ductility and toughness are too great to allow thorough examination of instability flow.

RECOMMENDATIONS FOR FUTURE WORK

1. The effect of dissolved hydrogen on the resolved shear stress of the hexagonal titanium lattice should be determined, as well as the effect of hydrogen on the number of active slip planes present.

2. The titanium alloy does not appear to be one that is easily tested for instability formation using sheet tensile specimens. Ernst[48] using the torsional mode of testing had shown that certain titanium alloys have no tolerance for instabilities. How much hydrogen was present in the material used for his tests is not known; nevertheless, in the present study it was illustrated that even with 150 ppm hydrogen there was some tolerance for the instabilities. It would thus be interesting to use the torsional mode of loading to examine the effect of hydrogen.

3. There is still some question as to whether hydrogen charged before testing has the ability to migrate anywhere in the lattice that the state of stress would dictate. For this reason the possibility of testing in a hydrogen atmosphere should be considered.

4. A more thorough investigation at still lower strain rates should be conducted using transmission microscopy to show the relationship of strain induced hydride to the instability strain parameters.

APPENDIX

SAMPLE CALCULATIONS FOR HYDROGENATION PROCEDURE

$PV = nRT$ (ideal gas law)

$$R = 62.5 \frac{\ell - \text{mmHg}}{\text{deg} - \text{mole}}$$

$$n = \frac{a}{M} = \frac{\text{g of gas}}{\text{molecular weight}} = \frac{\text{g of gas}}{2}$$

Since backfilling pressure was at room temperature,

$T = 273 + 23 = 296$ K

$$a = \text{amount of gas in g} = \frac{(\text{wt\%})(\text{sample wt})}{100} .$$

If one sample weighed 7.2 g then

$$P = \frac{nRT}{V} + \frac{a}{2} \times 62.5 \times \frac{296}{V} .$$

For a desired level of 250 ppm hydrogen with the initial hydrogen content 10 ppm, 240 ppm hydrogen must be added;

$$P = \frac{9250\ a}{V} = \frac{9250(.00173)}{V} .$$

If the volume of the charging capsule is measured to be 82.5 ml then $P = \frac{9250(.00173)}{.0825} = 194$ mmHG. Thus the charging pressure should be raised to 194 mmHg and then the capsule sealed.

REFERENCES

1. T. R. Beck, Proceedings of Conference on Fundamental Aspects of Stress Corrosion Cracking at The Ohio State University, R. W. Staehle, ed., NACE, Houston, 605, (1969).

2. D. T. Powell and J. C. Scully, Corrosion, 24, 151, (1968).

3. C. M. Chen, F. H. Beck, and M. G. Fontana, Corrosion, 27, 77, (1971).

4. J. A. S. Green and A. J. Sedricks, RIAS Technical Report 70-11C, Martin Marietta Corporation, October, 1970.

5. M. G. Fontana et al., "Corrosion Cracking of Metallic Materials," Technical Report AFML-69-16, The Ohio State University to Air Force Materials Laboratory, Wright-Patterson Air Force Base, Ohio, February, 1969.

6. B. F. Brown et al., "Marine Corrosion Studies," Third Interim Report of Progress, NRL Memorandum Report 1634, July, 1965.

7. "A Study of the Stress Corrosion Cracking of Titanium Alloys in Sea Water With Emphasis on the Ti-6Al-4V and Ti-8Al-1Mo-1V Alloys," Research Report No. R471, Project No. 93002, Reactive Metals, Inc., October 18, 1965.

8. M. H. Peterson, B. F. Brown, R. L. Newbegin and R. R. Groover, Corrosion, 23, 142, (1967).

9. J. D. Jackson and W. K. Boyd, "Stress-Corrosion and Accelerated Crack-Propagation Behavior of Titanium and Titanium Alloys," DMIC Technical Note, Battelle Memorial Institute, Feb. 1, 1966.

10. I. R. Lane, Jr., I. J. Cavallars, and A. G. S. Morton, "Sea-Water Embrittlement of Titanium," Stress-Corrosion Cracking of Titanium, ASTM STP 397, Am. Soc. Testing Mater., 1966, p. 246.

11. S. R. Seagle, R. R. Seeley, G. S. Hall, "The Influence of Composition and Heat Treatment on the Aqueous Stress Corrosion of Titanium," Research and Development Report 492, Reactive Metals, Inc., March 15, 1967.

12. I. R. Lane and J. L. Cavallart, "Metallurgical and Mechanical Aspects of Sea Water Stress Corrosion of Titanium," Applications Related Phenomena in Titanium Alloys, ASTM STP 432, 1968, p. 147.

13. R. A. Wood, J. D. Boyd, and R. I. Jaffee, "The Effect of Composition on the Salt Water Stress-Corrosion Susceptibility of Titanium Alloys Containing Aluminum, Molybdenum, Vanadium, and Oxygen," paper presented at the Second International Conference on Titanium Alloys, May 2-5, 1972.

14. R. A. Wood, J. D. Boyd, D. N. Williams, and R. I. Jaffee, "The Effect of Alloy Composition on the Mechanism of Stress-Corrosion Cracking of Titanium Alloys in Aqueous Environments," Annual Summary Report to NASA, June 11, 1971 to June 10, 1972.

15. E. L. Owen, F. H. Beck, and M. G. Fontana, "Stress Corrosion Cracking of Titanium Alloys," NASA Grant NGL 36-008-051, December, 1970.

16. I. R. Lane, J. L. Cavallero, and A. G. S. Morton, "Fracture Behavior of Titanium in the Marine Environment," MEL R&D Phase Report 231/65, U. S. Navy Marine Engineering Laboratory, Annapolis, Maryland, 1965.

17. R. C. May, F. H. Beck, and M. G. Fontana, "Stress Corrosion Cracking of Titanium Alloys" NASA Grant NGL 35-008-051, September, 1971.

18. P. Cotterill, "The Hydrogen Embrittlement of Metals," Progr. Mater. Sci. 9, No. 4, (1961).

19. J. G. Morlett, H. H. Johnson, A. R. Troiano, J. Iron Steel Inst. 37, (1958).

20. C. D. Beachem, "A New Model for Hydrogen-Assisted Cracking (Hydrogen "Embrittlement")" Met. Trans. 3, 437, (1972).

21. J. D. Boyd, "Precipitation of Hydrides in Titanium Alloys," Trans. Am. Soc. Metals, 62, 977, (1969).

22. D. N. Williams, "Hydrogen in Titanium Alloys," TML Report No. 100, May 16, 1958.

23. G. A. Lenning, J. W. Spretnak, R. I. Jaffee, "Effect of Hydrogen on Alpha Titanium Alloys," Trans. AIME, Oct., 1956.

24. G. A. Lenning, L. W. Berger and R. I. Jaffee, "The Effect of Hydrogen on Mechanical Properties of Titanium and Titanium Alloys," Fourth Summary Report from Battelle Memorial Institute to Watertown Arsenal Laboratory, Contract No. DAI-33-019-505-ORD-(P)-1, July 31, 1955.

25. D. N. Williams, F. R. Schwartzberg, P. R. Wilson, W. M. Albrecht, M. W. Mallett, and R. I. Jaffee, "Hydrogen Contamination in Titanium and Titanium Alloys, Part IV: The Effect of Hydrogen on the Hydrogen in Titanium Alloys," WADC TR-54-616, March, 1957.

26. J. D. Boyd, F. H. Haynie, W. K. Boyd, R. A. Wood, D. N. Williams, and R. I. Jaffee, "The Effect of Composition on the Mechanism of Stress-Corrosion Cracking of Titanium Alloys in N_2O_4 and Aqueous and Hot-Salt Environments," Fifth Quarterly Progress Report from Battelle Memorial Institute to the National Aeronautics and Space Administration, Contract No. NASr-100(09), February 29, 1968.

27. E. L. Owen, F. H. Beck, and M. G. Fontana, "Stress Corrosion Cracking of Titanium Alloys," Report No. 8, NASA Grant No. NGL-36-008-051, The Ohio State University Research Foundation, December, 1970.

28. R. Otsuka, "Studies on the Corrosion of Titanium," Scientific Papers, Inst. Phys. Chem. Res., 54, 97, (1960).

29. J. Spurrier and J. C. Scully, "Fractographic Aspects of the Stress Corrosion Cracking of Titanium in a Methanol/HCl Mixture," Corrosion, 28, No. 12, 453, (1972).

30. G. Sanderson and J. C. Scully, Corrosion Sci., 8, 541, (1968).

31. D. T. Powell and J. C. Scully, Corrosion, 25, 483, (1969).

32. J. C. Scully and D. T. Powell, Corrosion Sci., 10, 371, (1970).

33. D. A. Mauney, E. A. Starke, Jr., and R. F. Hockman, "Hydrogen Embrittlement and Stress Corrosion Cracking in Ti-Al Binary Alloys," Corrosion, 29, No. 6, 241, (1973).

34. V. J. Colangelo and M. S. Ferguson, "The Role of the Strain Hardening Exponent in Stress Corrosion Cracking of a High Strength Steel," Corrosion, 25, No. 12, 509, (1969).

35. C. D. Beachem, Trans. Am. Soc. Metals, 56, 318, (1963).

36. H. W. Hayden and S. Floreen, Acta Met., 17, 213, (1969).

37. A. K. Chakrabarti, "Characteristics of Plastic Instability in the Direction of Pure Shear," The Ohio State University, Ph.D. Dissertation, 1973.

38. R. H. Ernst and J. W. Spretnak, Trans. Iron Steel Inst. Japan, 9, No. 5, 361, (1969).

39. D. McGarry, The Ohio State University, M.S. Thesis, 1972.

40. N. H. Polakawski and S. Mostovy, Trans. Am. Soc. Metals, 54, 567, (1961).

41. Lo-Ching Chang, J. Mech. Phys. Solids, 3, (1955).

42. J. W. Spretnak, Trans. AIME, 236, 1639, (1966).

43. R. F. Recht, "Catastrophic Thermoplastic Shear," J. Appl. Mech., 189, (June 1964).

44. G. A. Lenning, J. Metals, 368, (March 1954).

45. M. J. Trzeciak, "Preparation and Analysis of Titanium-Hydrogen Standard Samples," DMIC, Memorandum 9, February 9, 1959.

46. J. F. Gloz, The Ohio State University, Ph.D. Dissertation, (to be published).

47. J. D. Boyd, P. J. Moreland, W. K. Boyd, R. A. Wood, D. N. Williams, and R. I. Jaffee, "The Effect of Composition on the Mechanism of Stress-Corrosion Cracking of Titanium Alloys in N_2O_4, and Aqueous and Hot-Salt Environments," Annual Report to NASA, Contract No. NASr-100(09), August 26, 1969, Battelle Memorial Institute.

48. R. H. Ernst, The Ohio State University, M.S. Thesis, 1967.

49. G. A. Lenning, M. S. Thesis, The Ohio State University, 1956.

50. J. D. Boyd, et al., (see Ref. 49), January, 1969.

51. A. T. Churchman, "The Slip Modes of Titanium and the Effect of Purity on Their Occurrence during Tensile Deformation of Single Crystals," Proc. Roy. Soc., A226, 216, (1954).

52. Shiro Kobayashi, Lecture Notes on Plasticity, Battelle Visiting Professor, The Ohio State University, 1967-68.

53. E. Parker, "Theory and Background of Fracture Mechanics," Chap. 1, Application of Fracture Toughness Parameters to Structural Metals, Metallurgical Society Conferences, Vol. 31, 1966.

54. F. R. Schwartzberg, The Ohio State University, M.S. Thesis, 1958.